Cell Biology, Developmental Biology

Reciprocal discoidin domain receptor signaling strengthens integrin adhesion to connect adjacent tissues

Kieop Park, Ranjay Jayadev, Sara G. Payne, Isabel W. Kenny-Ganzert, Qiuyi Chi, Daniel S. Costa, William Ramos-Lewis, Siddharthan Balachandar Thendral, David R. Sherwood

Department of Biology, Duke University, Box 90338, Durham, NC 27708, USA • Department of Cell Biology, Duke University Medical Center, Durham, NC 27708, USA

Reviewed Preprint

Revised by authors after peer review.

About eLife's process

Reviewed preprint version 2
June 12, 2023 (this version)

Reviewed preprint version 1
May 11, 2023

Posted to bioRxiv
March 15, 2023

Sent for peer review
March 14, 2023

Abstract

Separate tissues connect through adjoining basement membranes to carry out molecular barrier, exchange, and organ support functions. Cell adhesion at these connections must be robust and balanced to withstand independent tissue movement. Yet, how cells achieve synchronized adhesion to connect tissues is unknown. Here, we have investigated this question using the *C. elegans* utse-seam tissue connection that supports the uterus during egg-laying. Through genetics, quantitative fluorescence, and cell specific molecular disruption, we show that type IV collagen, which fastens the linkage, also activates the collagen receptor discoidin domain receptor 2 (DDR-2) in both the utse and seam. RNAi depletion, genome editing, and photobleaching experiments revealed that DDR-2 signals through LET-60/Ras to coordinately strengthen an integrin adhesion in the utse and seam that stabilizes their connection. These results uncover a synchronizing mechanism for robust adhesion during tissue connection, where collagen both affixes the linkage and signals to both tissues to bolster their adhesion.

eLife assessment

This **important** paper reveals how cells in adjacent tissues use the extracellular matrix to establish mechanical connections. Through a series of crisp genetic manipulations and quantitative image analyses, the authors provide **compelling** evidence to show how an essential adhesion between the uterus and the seam cells in the nematode *C. elegans* is formed. The assembly of type IV collagen triggers internalization of a cell surface receptor, which then signals from endocytic vesicles to strengthen the connection.

Introduction

Basement membrane (BM) is a planar, cell-associated extracellular matrix (ECM) that underlies or surrounds most tissues. BM provides tissues with structural support, barrier

functions, and signaling platforms (Morrissey and Sherwood 2015; Jayadev and Sherwood 2017; Hohenester and Yurchenco 2013). Type IV collagen provides BM with tensile strength, which allows BM to structurally support tissues and resist mechanical forces (Fidler, Boudko et al. 2018). Type IV collagen is a ligand for several vertebrate integrin receptors and the collagen-specific receptor tyrosine kinase discoidin domain receptor 1 (DDR1) (Khoshnoodi, Pedchenko et al. 2008; Brown, Cummings et al. 2017). Integrin and DDR1 interactions with type IV collagen mediate a wide variety cell-matrix functions, including cell migration and cell adhesion (Khoshnoodi, Pedchenko et al. 2008; Castro-Sanchez, Soto-Guzman et al. 2010; Borza and Pozzi 2014; Xiao, Jiang et al. 2015). DDR receptors and integrin also functionally interact within cells (Leitinger 2014); however, the roles of these interactions in native tissue settings remains poorly defined.

At tissue interfaces juxtaposed BMs usually slide along each other and maintain distinct tissue boundaries (Sherwood and Sternberg 2003; Brown 2011). At specific sites, however, the BMs of neighboring tissues link to stabilize tissue interactions and build complex organs (Keeley and Sherwood 2019). Examples include the kidney, where podocytes and endothelial BMs connect to form the glomerular BM blood filtration unit (Abrahamson 1985); the brain, where the astrocyte end feet and endothelial BMs join to build the blood-brain barrier (Sixt, Engelhardt et al. 2001); and the somite, where somite and epidermal BMs link to maintain somite-epidermal association during development (Feitosa, Zhang et al. 2012). Approximately 20 different BM-BM linkages between neighboring tissues have been documented (Gao, Mruk et al. 2017; Keeley and Sherwood 2019; Welcker, Stein et al. 2021). Disruption of these BM-BM tissue connections appear to underlie human diseases, such as in Alport's syndrome, where defects in kidney and hearing are associated with tissue linkage disruption (Merchant, Burgess et al. 2004; Naylor, Morais et al. 2021). Despite the prevalence and importance of BM-BM tissue connections, the challenge of studying tissue interactions *in vivo* has hampered our understanding of the mechanisms establishing and maintaining these linkages.

The simple tissues, visual transparency, and experimental tractability of *C. elegans* offers a powerful model to study BM-BM tissue interactions. Further, most *C. elegans* BM components and receptors are endogenously tagged with genetically encoded fluorophores to visualize localization, levels, and dynamics (Keeley, Hastie et al. 2020; Jayadev, Morais et al. 2022). A BM-BM tissue connection between the large, multinucleated uterine utse cell and epidermal seam cells stabilizes the uterus during egg laying. The utse-seam connection is formed by BMs of the utse and the seam cells, each ~50 nm thick, which are bridged by an ~100 nm connecting matrix (Vogel and Hedgecock 2001; Morrissey, Keeley et al. 2014; Gianakas, Keeley et al. 2023). Disruption of the utse-seam BM-BM tissue linkage results in prolapse of the uterus (**Rup**tured phenotype) out of the animal after the onset of egg-laying. Formation of the utse-seam attachment is initiated by the deposition of the matrix proteins fibulin and hemicentin during the last larval stage of development. Hemicentin promotes the recruitment of type IV collagen, which accumulates at high levels at the BM-BM tissue connection and strengthens the adhesion, allowing it to resist the strong mechanical forces of egg-laying. The utse-seam connection is robust, with each component of the tissue-spanning matrix contributing to the BM-BM connection (Gianakas, Keeley et al. 2023). This likely accounts for the ability of the utse-seam connection to initially resist mechanical forces after loss of any of these components, delaying the uterine prolapse phenotype until sometime after the initiation of egg-laying. The integrin, αINA-1, one of two *C. elegans* alpha integrins, is also expressed in the utse and is required to prevent uterine-prolapse during egg-laying. However, its regulation and function at the utse-seam connection is unclear (Morrissey, Keeley et al. 2014; Gianakas, Keeley et al. 2023). Mechanisms that link juxtaposed BMs appear to be shared, as hemicentin-1 promotes BM-BM tissue connection in the zebrafish fin fold, hemicentin-2 and fibulin-1 mediate zebrafish somite-epidermis BM-BM association, and hemicentin-1 stabilizes BM-BM linkage at myotendinous junctions in mice

(Carney, Feitosa et al. 2010; Feitosa, Zhang et al. 2012; Welcker, Stein et al. 2021). In addition, type IV collagen bridges the podocyte BM and endothelial BM to form the glomerular BM in mice and humans (Suleiman, Zhang et al. 2013; Naylor, Morais et al. 2021). While significant insights are being gained on matrix composition at BM-BM tissue connections, it remains unknown how tissues coordinate and strengthen their adhesive activity at linkage sites. Cells at tissue connections must resist the forces of tissue shifting arising from growth, muscle contraction, and blood flow, and it is unclear how tissues synchronize and bolster adhesions at tissue linkage sites.

Here, we discover that the *C. elegans* discoidin domain receptor DDR-2, an ortholog to the two vertebrate collagen binding DDR tyrosine kinase receptors (RTK), coordinates and strengthens an integrin mediated cell adhesion to support the utse-seam BM-BM tissue linkage during its formation. Using genetics, endogenous tagging, and tissue-specific molecular perturbations, we show that DDR-2 is expressed and functions in the utse and seam cells to mediate utse-seam attachment between the mid and late L4 larval stages. We reveal that assembly of type IV collagen linking the juxtaposed BMs triggers the internalization of DDR-2 in both the utse and seam cells into endocytic vesicles, a signaling compartment for DDR/RTK receptors. In the *ddr-2* knockout mutant, gaps in utse-seam attachment occurred at this time. Through tissue-specific perturbation, quantitative fluorescence analysis, and fluorescence recovery after photobleaching (FRAP), we provide evidence that DDR-2 signals through LET-60/Ras to increase the levels and stability of the α-integrin INA-1 at the utse-seam linkage. Together, these results reveal a mechanism for synchronizing a robust adhesion during tissue linkage, where type IV collagen, which bridges and fastens the BM-BM tissue linkage, also serves as a signal to coordinate, and bolster cell-matrix adhesion in cells on both sides of the tissue connection.

Results

The utse and seam cells associate during the early-L4 stage

The utse is an H-shaped syncytial uterine cell that underlies the *C. elegans* uterus and opens along the central crossbar region during egg-laying to allow embryo passage (Ghosh and Sternberg 2014). The utse is flanked laterally on both sides of the animal by a string of epidermal seam cells that run the length of the body. The utse cell and seam cells are each encased in a BM, which become linked by a specialized matrix whose known functional components include hemicentin, fibulin, and type IV collagen (***Figure 1A***) (Gianakas, Keeley et al. 2023). The BM-BM tissue connection supports the uterus during egg-laying and disruption of the linkage results in uterine prolapse (***Figure 1B and C***) (Vogel and Hedgecock 2001). The utse and seam cells are in contact by the mid L4 larval stage (Gianakas, Keeley et al. 2023), but when the initial contact is established is not known.

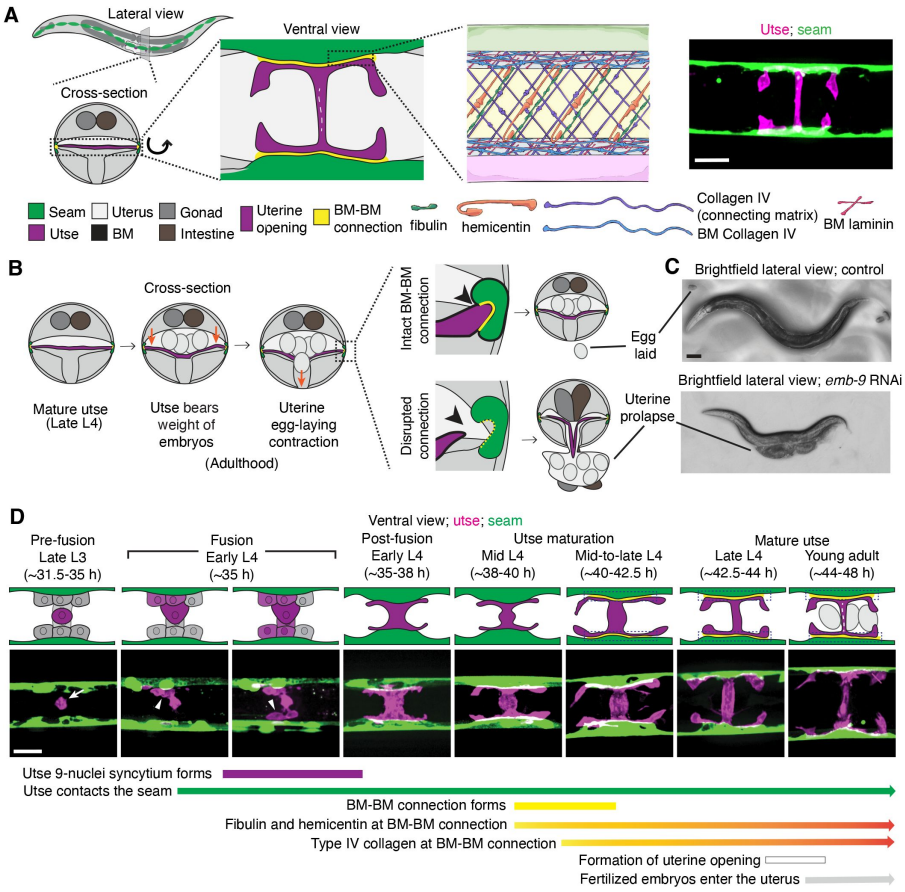

Figure 1

Morphogenesis of the *C. elegans* utse-seam basement membrane-basement membrane tissue connection.

(**A**) Left and center: Schematic depicting the utse-seam connection. The utse (a syncytial uterine cell) and the seam epidermal cells are both encased in basement membranes (BMs), which are linked by a BM-BM connecting matrix. Right: ventral fluorescence z-projection showing the utse and seam cells visualized by the markers *cdh-3p::mCherry::PLC*$^{\delta PH}$ and *scmp::GFP::CAAX*, respectively. (**B**) Schematic illustrating the role of the utse-seam connection in supporting the uterus during egg-laying muscle contractions. Disruption of the connection results in uterine prolapse. (**C**) Lateral brightfield images of adult worms on control RNAi treatment or RNAi against a key component of the BM-BM linkage, α1 type IV collagen/*emb-9* (RNAi fed from the L1 onward); note the uterine prolapse after loss of collagen. (**D**) A schematic summarizing the development of the utse-seam connection. Fluorescence images shown are ventral z-projections of the utse and the seam at the respective developmental stages from the late L3 to young adult (hours post-hatch at 20°C). Arrow indicates the uterine anchor cell (AC) that fuses with adjacent uterine cells to form the utse. During syncytium formation, the utse makes contact with the seam cells (arrowheads). Dotted boxes denote the BM-BM connection. Scale bars, 20 μm.

The utse is formed from the fusion of one specialized uterine cell, the anchor cell, with eight adjacent uterine pi cell progeny, forming the syncytial nine-nuclei utse during the early L4 stage (Newman, White et al. 1996; Ghosh and Sternberg 2014). To determine when the utse first contacts the seam cells, we used an anchor cell-specific mCherry fluorophore marker (*cdh-3p::mCherry::PLCδ*^{PH}; ***Figure 1D***, arrow) (Hagedorn, Yashiro et al. 2009) that diffuses into the uterine pi cell progeny during fusion and simultaneously viewed a GFP seam cell marker (*scmp::GFP::CAAX*) (Chapman, Li et al. 2008). We found that the utse contacts the seam cells during the early L4 stage as the utse syncytium forms (***Figure 1D***, arrowheads; n=5/5 cases observed). Shortly after utse-seam contact, the BM-BM linkage is initiated at the mid L4 stage by the assembly of low levels of hemicentin, which is secreted by the utse and fibulin-1, which hemicentin recruits from the extracellular fluid. Fibulin-1 and hemicentin protect the utse-seam cell connection from mechanical forces arising from body movement and uterine and vulval muscle contractions prior to egg-laying (Gianakas et al. 2023). Hemicentin also promotes recruitment of type IV collagen from the extracellular fluid, which allows the utse-seam BM-BM connection to resist the strong mechanical forces from egg-laying (Gianakas et al. 2023) (***Figure 1D***). Together, these results show that the utse and seam cells are in contact

prior to deposition of matrix components that strengthen the utse-seam BM-BM tissue connection.

Loss of discoidin domain receptor-2 (DDR-2) causes uterine prolapse

As type IV collagen is critical to the BM-BM connection, we were next interested in understanding how receptors for type IV collagen regulate the utse-seam BM-BM linkage. The two main receptors for type IV collagen are integrin and the discoidin domain receptor (DDR) (Fidler, Boudko et al. 2018). *C. elegans* harbor two integrin heterodimers composed of different α chains with a shared β chain: αINA-1/ βPAT-3 and αPAT-2/ βPAT-3 (Clay and Sherwood 2015). The integrin INA-1 is expressed in the utse and its loss leads to uterine prolapse, suggesting a possible role in utse-seam attachment (Morrissey, Keeley et al. 2014; Gianakas, Keeley et al. 2023). Whether DDRs function at the utse-seam connection, however, is unknown.

C. elegans have two DDR genes, *ddr-1* and *ddr-2*, which are paralogs and orthologs to the two mammalian DDRs (Vogel, Abdulhussein et al. 2006). Like mammalian counterparts, the *C. elegans* DDRs are comprised of discoidin and discoidin-like domains, followed by a transmembrane domain and a kinase domain (***Figure 2A***). To determine if *C. elegans* DDRs play a role in utse-seam BM-BM linkage, we examined several *ddr-1* and *ddr-2* mutants (***Figure 2A***). We first screened for the Rup phenotype caused by uterine prolapse, observing animals every day during the egg-laying period, from its onset (48 h post-L1) to end (120 h) (***Methods***). Animals harboring the *ddr-1(ok874)* deletion allele, which eliminates the intracellular portion of DDR-1, and animals with the *ddr-1(tm382)* allele containing an early stop codon truncating the majority of the predicted protein (Unsoeld, Park et al. 2013), did not show a Rup phenotype (***Figure 2A and B***). In contrast, animals homozygous for the *ddr-2(tm797)* allele, which introduces an early stop codon and is thought to be a null or strong loss-of-function (Unsoeld, Park et al. 2013), exhibited a significant Rup/uterine prolapse defect. Animals carrying the *ddr-2(ok574)* allele, which deletes a portion of the intracellular kinase domain (Unsoeld, Park et al. 2013), also showed an increased frequency of the Rup phenotype compared to wild-type animals, although this difference was not statistically significant (***Figure 2A and B***). We further generated a full-length *ddr-2* deletion allele, *ddr-2(qy64)*, and confirmed that complete loss of *ddr-2* led to a significant uterine prolapse defect (***Figure 2A and B***). Taken together, these results indicate that DDR-2 protects against uterine prolapse and may play a role in mediating utse-seam BM-BM attachment.

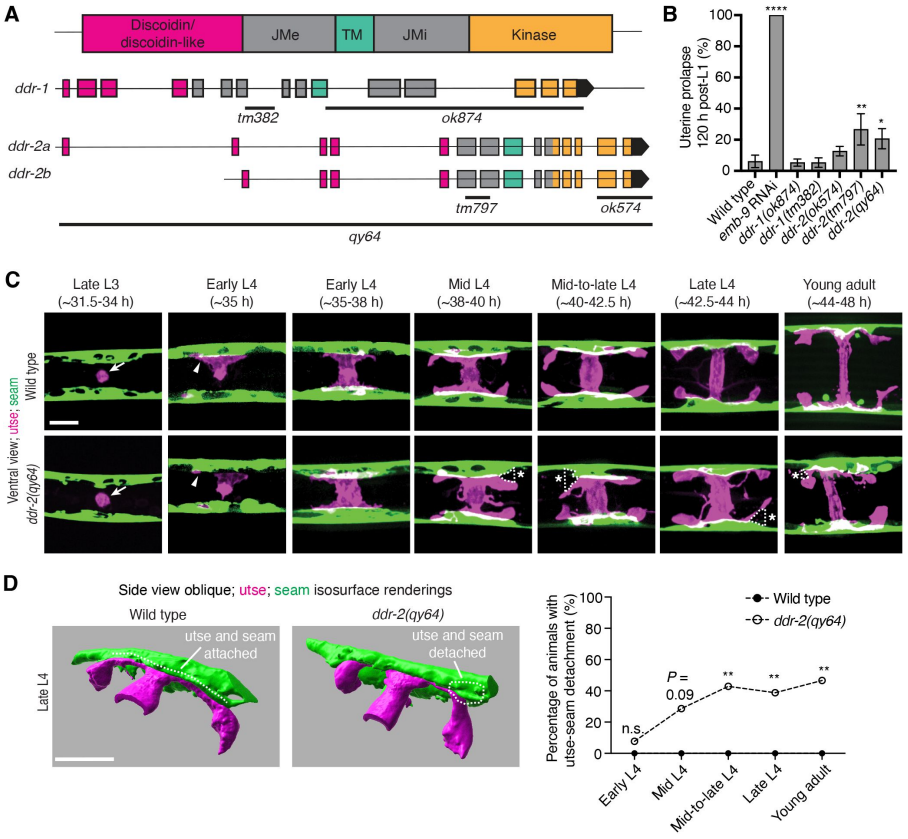

Figure 2 with 1 supplement

DDR-2 promotes utse-seam attachment and protects against uterine prolapse.

(A) Domain structure of *C. elegans* discoidin domain receptors (DDRs) and exon-intron gene structures of *ddr-1* and *ddr-2*. Exons are color coded according to respective domains. Gene regions that are deleted in respective mutant alleles (italicized text) are demarcated by solid black lines. (**B**) Frequency of uterine prolapse in *ddr-1* and *ddr-2* mutant animals compared to wild type 120 h post-L1 plating. Data are shown as mean prolapse percentage ± SD, derived from three independent trials (n = 50 animals screened per trial). α1 type IV collagen/*emb-9* RNAi was used as a positive control. ****$P \leq 0.0001$, **$P \leq 0.01$, *$P \leq 0.05$; one-way ANOVA with post hoc Dunnett's test. (**C**) Ventral fluorescence z-projections of the utse *(cdh-3p::mCherry::PLC$^{\delta PH}$)* and seam *(scmp::GFP::CAAX)* cells in wild-type and *ddr-2* knockout *(ddr-2(qy64))* animals from the late L3 to young adult developmental stages (hours post-hatch at 20°C). Arrows indicate the AC prior to utse formation and arrowheads denote early contacts between the utse and seam. Dotted lines with asterisks indicate regions of utse-seam detachment in *ddr-2(qy64)* animals. (**D**) Left: 3D isosurface renderings of the utse and seam in representative late L4 wild-type and *ddr-2(qy64)* animals (see also ***Figure 2—video 1***). Right: Quantification of the percentage of animals with utse-seam detachment. Wild type, early L4 to young adult: n = 0/13, n = 0/14, n = 0/22, n = 0/21, n = 0/18 animals with detachments respectively; *ddr-2(qy64)*, early L4 to young adult: n = 1/13, n = 4/14, n = 9/22, n = 7/18, n = 7/15 animals with detachments respectively. **$P \leq 0.01$, n.s. (not significant), $P > 0.05$; Fisher's exact test. Scale bars, 20 μm.

Source data 1. Source data for ***Figure 2***. Raw data of uterine prolapse frequency used to generate ***Figure 2B*** in Microsoft Excel format.

Figure 2—video 1. Animation of 3D isosurface rendering of the utse and seam in a representative late L4 wild-type animal; related to ***Figure 2D***.

DDR-2 maintains utse-seam attachment during formation of the tissue connection

To determine if the Rup phenotype observed in *ddr-2* mutants is a result of perturbations in the utse-seam BM-BM tissue connection, we examined utse-seam association from the late L3 through young adult stages in animals harboring the *ddr-2*(*qy64)* deletion allele (***Figure 2C***). We visualized utse-seam association using the utse and seam cell membrane markers *cdh-3p::mCherry::PLCδ^{PH}* and *scmp::GFP::CAAX*, respectively. Animals homozygous for *ddr-*

2(qy64) had normal utse-seam cell association at the early L4 stage; however, beginning at the mid L4 stage, gaps in the utse-seam attachment were detected in about 30% of animals. The frequency of gaps increased to ~40% of animals by the mid-to-late L4 and persisted at a similar penetrance to young adulthood (***Figure 2C and D***). In addition, membrane projections emanating from the central body of the utse were detected in *ddr-2(qy64)* animals. These projections were first observed at the mid L4 stage and persisted to young adulthood (***Figure 2C***). These observations suggest that DDR-2 functions around the mid L4 to late L4 stages to promote utse-seam attachment, and that DDR-2 may also regulate utse morphology. Next, we wanted to determine if the utse-seam detachment observed in *ddr-2(qy64)* mutants led to uterine prolapse. Wild-type and *ddr-2(qy64)* animals were mounted and imaged at the L4 larval stage for utse-seam attachment defects, recovered, and tracked to the 72-hour adult stage, where they were examined for the Rup phenotype. All wild-type L4 larvae had intact utse-seam attachment and did not rupture by 72-hour adulthood (n=8/8 animals). However, among nine *ddr-2(qy64)* mutant animals examined, four exhibited utse-seam detachments at the L4 stage, all of which underwent uterine prolapse (Rup) by adulthood. The remaining five *ddr-2* mutant animals, which had an intact utse-seam linkage, did not display the Rup phenotype. Taken together, these results suggest that DDR-2 promotes utse-seam attachment during early stages of tissue linkage.

DDR-2 is found within endocytic vesicles in the utse and seam cells during initial stages of tissue attachment

As utse-seam detachment in *ddr-2* mutant animals was first observed at the mid L4 larval stage, we next sought to determine if DDR-2 was expressed in the utse, seam, or both cell types at this time. Between the mid L4 and late L4 stage, the utse-seam tissue connection forms into a tongue-and-groove association between the utse (tongue) and seam (groove) (***Figure 2D and Figure 2—video 1***). To resolve whether DDR-2 is localized within the seam, utse, or both (Vogel and Hedgecock 2001), we used either a utse (*cdh-3p::mCherry::PLC*δ^{PH}) or seam cell marker (*scmp::2xmKate2::PLC*δ^{PH}), and imaged endogenously tagged DDR-2 protein (DDR-2::mNG) (Keeley, Hastie et al. 2020) in lateral confocal sections from the L4 to young adult stages (***Figure 3A***). We first examined the seam cells contacting the utse (***Figure 3B***). At the early L4 stage DDR-2::mNG was faintly visible at the surface of the seam cells and found in a few intracellular punctae (***Figure 3B***, n=10/10 animals). By the mid L4 stage, DDR-2 was predominantly found in punctae in the region of attachment with the utse. Levels of punctae increased until the late L4 stage and then declined sharply by the young adult (***Figure 3B***). Notably, at the late L4, when DDR-2 punctate localization was at its highest, we could not detect any DDR-2 signal at the cell surface (***Figure 3B***, n = 9/9). We further examined DDR-2::mNG in seam cells that were not contacting the utse and found that DDR-2 levels were uniformly low from the early L4 through the young adult stages (***Figure 3—figure supplement 1A***). We next investigated DDR-2 localization in the utse contacting the seam. Like the seam cells at the tissue connection site, DDR-2 in the utse was punctate and peaked in levels between the mid and late L4 stages and then declined rapidly (***Figure 3C***). We conclude that DDR-2 is present at high levels and localized within punctate structures in the seam and utse cells at the time when utse-seam defects are observed in *ddr-2* mutant animals.

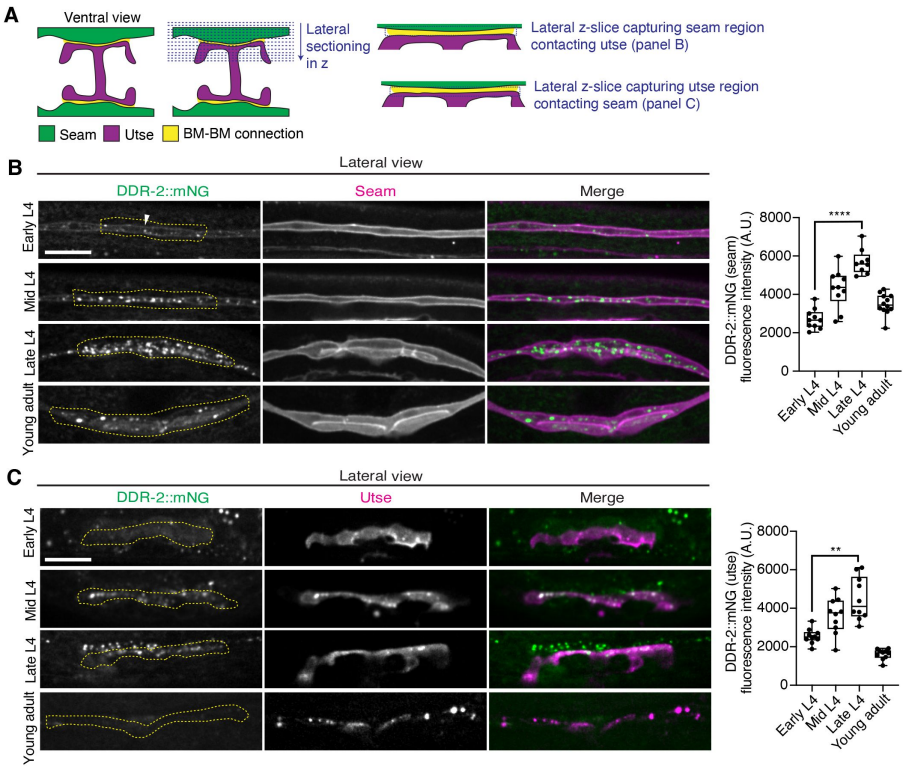

Figure 3 with 1 supplement

DDR-2 levels peak in the utse and seam during the formation of the BM-BM connection.

(**A**) Schematic illustrating lateral z-sectioning to determine slices that capture the seam region in contact with the utse and vice-versa. (**B**) Left: Lateral fluorescence images of DDR-2::mNG visualized with the seam marker *scmp::2xmKate2::PLC*$^{\delta PH}$ from the early L4 to young adult stages. Dotted yellow regions indicate DDR-2 signal in the seam contacting the utse. White arrowhead denotes DDR-2 signal at the cell surface. Right: Quantification of mean DDR-2::mNG fluorescence intensity in the dotted regions (n ≥ 9 for each developmental stage). ****$P \leq 0.0001$, one-way ANOVA with post hoc Dunnett's test. (**C**) Left: Lateral fluorescence images of DDR-2::mNG visualized with the utse marker *cdh-3p::mCherry::PLC*$^{\delta PH}$ from the early L4 to young adult stages. Dotted yellow regions indicate DDR-2 signal in the utse contacting the seam. Right: Quantification of mean DDR-2::mNG fluorescence intensity in dotted yellow regions (n = 10 all stages). **$P \leq 0.01$, one-way ANOVA with post hoc Dunnett's test. Scale bars, 20 µm. Box edges in boxplots represent the 25th and 75th percentiles, the line in the box denotes the median value, and whiskers mark the minimum and maximum values.

Source data 1. Source data for ***Figure 3***. Raw data of DDR-2::mNG fluorescence intensity quantification in the seam and utse used to generate boxplots in ***Figure 3B and C*** in Microsoft Excel format. Note that the boxplot in ***Figure 3—figure supplement 1A*** was also generated from these data. **Source data 2.** Source data for ***Figure 3—figure supplement 1***. Raw data of DDR-2::mNG and mCherry-tagged vesicle marker co-localization analysis used to generate boxplots in ***Figure 3—figure supplement 1B and C*** in Microsoft Excel format.

Figure supplement 1. DDR-2 is found within endocytic vesicles; related to ***Figure 3B and C***.

Receptor tyrosine kinases (RTKs), including DDRs, are activated upon ligand binding and then rapidly internalized into endocytic vesicles: first the early endosome (marked by RAB-5), followed by subsequent sorting for either lysosome-mediated degradation via late endosomes (marked by RAB-7), or recycled back to the cell surface in recycling endosomes (marked by RAB-11) (Goh and Sorkin 2013). In vertebrates, the exposure of cells to collagen results in the internalization of DDR1b into Rab5a positive early endosomes (Mihai, Chotani et al. 2009). Phosphorylation of DDR1 does not occur until the onset of endocytosis and recycling, suggesting that receptor activation occurs in endocytic vesicles ((Mihai, Chotani et al. 2009), Fu, Valiathan et al. 2013). As *C. elegans* DDR-2 appeared to be functioning during the mid L4 to late L4 stages, when levels of DDR-2 were highest and present in vesicular structures, we sought to determine whether DDR-2 was internalized within endocytic vesicles. We examined localization of DDR-2::mNG punctae in relation to utse-expressed

markers of early endosomes (*cdh-3p::mCherry::rab-5*), late endosomes (*cdh-3p::mCherry::rab-7*), and recycling endosomes (*cdh-3p::mCherry::rab-11*) (Sato, Norris et al. 2014). DDR-2 was co-localized with all three classes of endosomes in the utse, with the highest overlap with RAB-5 early endosomes (***Figure 3—figure supplement 1B***). In addition, we examined an early endosome marker expressed in seam cells (*scmp::mKate2::rab-5*) and observed DDR-2::mNG punctae co-localized with RAB-5 vesicles (***Figure 3—figure supplement 1C***). The presence of DDR-2 in endocytic vesicles within the utse and seam suggested that DDR-2 signaling may be required for utse-seam attachment. Consistent with this, animals harboring the *ddr-2(ok574)* mutant allele, where a portion of the intracellular kinase domain is deleted (***Figure 2A***), exhibited significant utse-seam detachments at the late L4 stage (***Figure 4A***). Taken together, these observations suggest that DDR-2 functions in the utse and seam cells to promote attachment at the tissue linkage site between the mid and late L4 stages, where it may signal within endocytic vesicles.

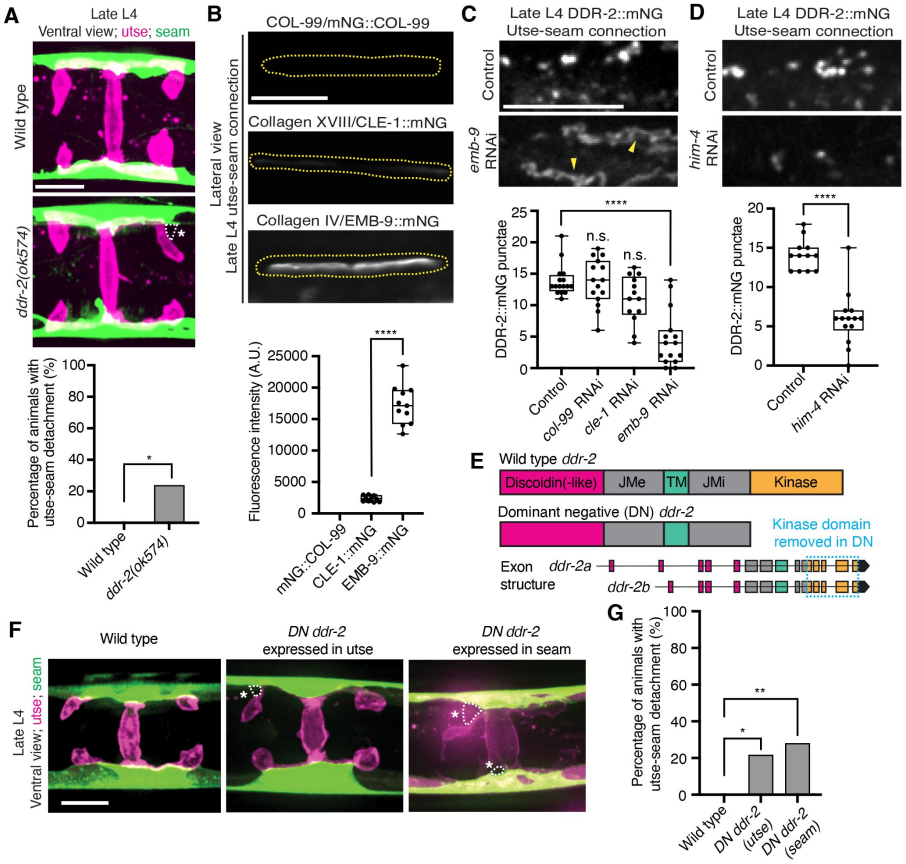

Figure 4 with 1 supplement

DDR-2 endocytosis is triggered by type IV collagen and DDR-2 is required in both the utse and seam to promote tissue connection.

(A) Top: Ventral fluorescence z-projections of the utse *(nas-22p::2xmKate2::PLC$^{\delta PH}$)* and seam *(scmp::GFP::CAAX)* cells in late L4 wild-type and *ddr-2* kinase domain truncation mutant *(ddr-2(ok574))* animals. Dotted lines with asterisks indicate regions of utse-seam detachment. Bottom: Quantification of the percentage of animals with utse-seam detachment. Wild type, n = 0/26; *ddr-2(ok574)*, n = 5/21 animals with detachments respectively. ***P* ≤ 0.01, Fisher's exact test.

(B) Top: Lateral fluorescence images of COL-99 (mNG::COL-99), type XVIII collagen (CLE-1::mNG), and α1 type IV collagen (EMB-9::mNG) at the utse-seam connection (dotted yellow regions) of late L4 animals. All images were acquired at the same exposure. Bottom: Quantification of mean fluorescence intensity (n ≥ 10 for each fluorescent protein). *****P* ≤ 0.0001, unpaired two-tailed Student's *t* test. (**C**) Top: Lateral fluorescence z-projections of DDR-2::mNG at the utse-seam connection in control or *emb-9* RNAi-treated late L4 animals. Note that the field of view contains a single utse arm contacting the seam tissue. Arrowheads indicate cell surface accumulation of DDR-2 upon collagen IV depletion. Bottom: Quantification of the average number of discrete DDR-2 punctae at the utse-seam connection on control, *col-99*, *cle-1*, or *emb-9* RNAi treatments (n ≥ 13 animals for all treatments). *****P* ≤ 0.0001, n.s. (not significant), *P* > 0.05; Kruskal-Wallis *H* test with post hoc Dunn's test. (**D**) Top: Lateral fluorescence z-projections of DDR-2::mNG at the utse-seam attachment in control or hemicentin/*him-4* RNAi-treated late L4 animals. Bottom: Quantification of the average number of discrete DDR-2 punctae at the utse-seam attachment on control or *him-4* RNAi-treated animals (n ≥ 13 all treatments). *****P* ≤ 0.0001, Mann-Whitney *U* test. (**E**) Schematic of dominant negative (DN) *ddr-2*. (**F**) Ventral

fluorescence z-projections of the utse *(nas-22p::2xmKate2::PLC$^{\delta PH}$)* and seam *(wrt-2p::GFP::PLC$^{\delta PH}$)* tissues in late L4 stage wild-type animals and animals expressing *DN ddr-2* in the utse (driven by *cdh-3* promoter) or the seam (driven by *scm* promoter). Dotted lines with asterisks indicate regions of utse-seam detachment. (**G**) Quantification of the percentage of animals with utse-seam detachment. Wild type, n = 0/23; *DN ddr-2(utse)*, n = 5/23; *DN ddr-2(seam)*, n = 7/25 animals with detachments respectively. $^{**}P \leq 0.01$, $^{*}P \leq 0.05$; Fisher's exact test. Scale bars, 20 µm. Box edges in boxplots represent the 25th and 75th percentiles, the line in the box denotes the median value, and whiskers mark the minimum and maximum values.

Source data 1. Source data for Figure 4. Raw data of fluorescence intensity quantification of tagged collagen ligands at the utse-seam connection used to generate boxplot in ***Figure 4B***, and raw data of DDR-2::mNG puncta counts at the utse-seam connection upon collagen ligand or hemicentin depletion used to generate boxplots in ***Figure 4C and D*** in Microsoft Excel format.

Source data 2. Source data for ***Figure 4—figure supplement 1***. Raw data of quantification of knockdown efficiencies of tagged collagen ligands and hemicentin at the utse-seam connection used to generate boxplots in ***Figure 4—figure supplement 1*** in Microsoft Excel format.

Figure supplement 1. Collagen and hemicentin knockdown efficiencies; related to ***Figure 4C and D***.

Type IV collagen promotes DDR-2 vesiculation

DDR signaling is triggered by collagen binding, and vertebrate DDRs bind multiple collagens with different binding affinities (Leitinger 2014). Genetic interaction studies in *C. elegans* revealed that transmembrane collagen COL-99, which is most similar to transmembrane collagen type XIII, XXIII, and XXV in vertebrates (Tu, Huhtala et al. 2015), may act as a ligand for *C. elegans* DDR-1 and DDR-2 during axon guidance and that type IV collagen might act as a ligand for DDR-2 during axon regeneration (Hisamoto, Nagamori et al. 2016; Taylor, Unsoeld et al. 2018). *C. elegans* BMs also harbor type XVIII collagen (CLE-1) (Keeley, Hastie et al. 2020). Thus, we next investigated whether any of these cell and BM-associated collagens could function as a ligand for DDR-2 at the utse-seam BM-BM tissue connection site.

Type IV collagen enriches at the utse-seam BM-BM linkage during its maturation and helps the connected tissues resist the mechanical forces of egg-laying. In contrast, type XVIII collagen is not present enriched at the linkage (Gianakas, Keeley et al. 2023). Whether COL-99 localizes to the utse-seam tissue linkage is unknown. We thus first examined an endogenously tagged COL-99 (mNG::COL-99) (Jayadev, Morais et al. 2022) and compared its localization and levels to type IV collagen (α1-type IV collagen::mNG (EMB-9::mNG)) and type XVIII collagen (CLE-1::mNG) (Keeley, Hastie et al. 2020) at the utse-seam connection in late L4 animals. COL-99 was not detected while EMB-9 was present at nearly 8-fold higher levels than CLE-1, suggesting that type IV collagen might be the ligand for DDR-2 (***Figure 4B***). Furthermore, the enrichment of type IV collagen levels at the utse-seam connection site occurs rapidly from the mid L4 to late L4 stage (Gianakas, Keeley et al. 2023), correlating with the buildup of DDR-2 in endosomes in the utse and seam cells.

As exposure to collagen triggers vesiculation of vertebrate DDR1b into endocytic vesicles, we wanted to determine whether type IV collagen controls vesiculation of DDR-2 at the utse-seam BM-BM connection. RNAi-mediated depletion of type IV collagen from the L1 through the late L4 larval stages resulted in a sharp decrease in vesicular DDR-2::mNG in the utse and seam cells at the linkage site, accompanied by enrichment of DDR-2 at cell surfaces (***Figure 4C***; ***Figure 4—figure supplement 1A***). In contrast, reduction of COL-99 and type XVIII collagen did not significantly affect DDR-2 vesiculation (***Figure 4C***; ***Figure 4—figure supplement 1B and C***). Depletion of hemicentin, which plays a crucial role in recruiting type IV collagen to the

BM-BM linking matrix (Gianakas, Keeley et al. 2023), also resulted in a significant reduction in DDR-2 vesiculation (***Figure 4D***; ***Figure 4—figure supplement 1D***). In addition, we did not detect DDR-2 at the cell surface, suggesting that hemicentin has a role in recruiting DDR-2 to the site of utse-seam attachment. It is possible that collagen could also function in DDR-2 recruitment, but we could not assess this definitively due to the lower knockdown efficiency of *emb-9* RNAi (***Figure 4—figure supplement 1A***). Together, these findings indicate that type IV collagen assembly at the site of utse-seam BM-BM tissue linkage triggers DDR-2 vesiculation and may act as a ligand for DDR-2 activation to promote utse-seam attachment.

DDR-2 functions in the utse and the seam to promote utse-seam attachment

Since DDR-2 localizes to both the utse and seam cells, we next investigated where DDR-2 functions to promote utse-seam BM-BM attachment. We generated genome edited lines with single-copy insertions of dominant negative (DN) *ddr-2* (Bernadskaya, Brahmbhatt et al. 2019) driven by the *cdh-3* promoter for utse expression or the *scm* promoter for seam expression. Using the utse-specific membrane marker (*nas-22p::2xmKate2::PLC*δ^{PH}) (Park, Pan et al. 2010) and a seam cell membrane marker (*wrt-2p::GFP::PLC*δ^{PH}) (Wildwater, Sander et al. 2011), we found significant utse-seam detachments in both utse-expressed and seam-expressed *DN ddr-2* animals at the late L4 stage (***Figure 4F and G***). Consistent with the timing and vesicular pattern of DDR-2 localization, these results indicate that DDR-2 functions in both the utse and seam between the mid and late L4 stages to promote utse-seam attachment.

Loss of DDR-2 increases type IV collagen at the utse-seam BM-BM adhesion site

The matrix components fibulin-1 and hemicentin play early roles in mediating utse-seam attachment and hemicentin promotes recruitment of type IV collagen and further enrichment of fibulin, which strengthens the BM-BM attachment (Gianakas et al. 2023). We thus next asked whether DDR-2 promotes utse-seam linkage by regulating the assembly of fibulin, hemicentin, or type IV collagen at the connecting matrix. Knockdown of *ddr-2* by RNAi did not alter fibulin levels at the late L4 stage (***Figure 5—figure supplement 1A and B***). However, we observed a modest ~20% reduction in hemicentin upon depletion of DDR-2 (***Figure 5—figure supplement 1C***). As loss of hemicentin results in utse-seam detachment at the late L4 stage (Gianakas, Keeley et al. 2023), we tested whether a ~20% reduction of hemicentin could cause these defects by initiating RNAi at the early L4, just before the utse forms (***Methods***). We found that utse-seam attachments were intact in all animals at the late L4 stage upon ~20% reduction of hemicentin (n=13/13 and 12/12 control and *him-4* RNAi-treated animals examined respectively; ***Figure 5—figure supplement 1D***), suggesting that the utse-seam detachment defect in *ddr-2* mutant animals is not caused by a modest reduction in hemicentin levels. Interestingly, there was an ~40% increase in type IV collagen levels at the utse-seam connection after RNAi mediated reduction of *ddr-2*, indicating a possible feedback mechanism between DDR-2 signaling and collagen assembly (***Figure 5—figure supplement 1E***). In sum, these results indicate that knockdown of *ddr-2* does not decrease the functional levels of key matrix components at the site of utse-seam BM-BM connection, suggesting that DDR-2 does not promote utse-seam attachment by regulating the assembly of the BM-BM linking matrix.

DDR-2 promotes integrin function to mediate utse-seam tissue attachment

Studies have indicated that vertebrate DDRs are not strong adhesive receptors (Xu, Bihan et al. 2012). Consistent with this, we detected weak DDR-2::mNG fluorescence signals at the cell membranes of the utse and seam. However, we observed strong DDR-2 signals in a vesicular pattern in both tissues. We thus assessed several molecular activities regulated by DDR signaling that might mediate utse-seam attachment. Vertebrate DDRs promote matrix metalloproteinase (MMP) expression and localization (Leitinger 2014). The *C. elegans* genome harbors six MMP genes, named zinc metalloproteinase 1-6 (*zmp-1-6*) (Altincicek, Fischer et al. 2010). We examined four available reporters of ZMP localization (ZMP-1::GFP, ZMP-2::GFP, ZMP-3::GFP, and ZMP-4::GFP) (Kelley, Chi et al. 2019). Only ZMP-4 was detected at the utse-seam connection and its localization was not altered by knockdown of *ddr-2* (***Figure 5—figure supplement 1F***). These observations suggest that DDR-2 does not promote utse-seam linkage through regulation of MMPs, although we cannot rule out roles for DDR-2 in promoting the expression or localization of ZMP-5 or ZMP-6.

DDRs also modulate integrin activity (Leitinger 2014). Cell culture studies have shown that vertebrate DDRs can enhance integrin adhesion and integrin cell surface levels in multiple cell types (Xu, Bihan et al. 2012; Staudinger, Spano et al. 2013; Bayer, Grither et al. 2019). *C. elegans* harbor only two integrin receptors, made up of either the α subunit INA-1 or PAT-2 dimerized to the sole β subunit PAT-3 (Clay and Sherwood 2015). We previously found that depletion of INA-1 results in a Rup phenotype, but the specific effect on utse-seam BM-BM tissue attachment was not determined (Morrissey, Keeley et al. 2014). Thus, we next asked whether DDR-2 promotes utse-seam attachment through regulation of integrin. First, we analyzed the localization and levels of endogenously tagged INA-1 (αINA-1::mNG) and PAT-2 (αPAT-2::2xmNG) (Jayadev, Chi et al. 2019) and found that both integrin α subunits were expressed in the utse and seam tissues and localized to the utse-seam connection region from the mid-L4 stage through young adulthood (***Figure 5A and B***; ***Figure 5—figure supplement 2A and B***). Their levels mirrored that of DDR-2, with a peak at the late L4 stage, followed by a drop off in the young adult stage (***Figure 5A and B)***. However, lNA-1 levels were at least sixfold greater than PAT-2 (note, each PAT-2 is linked to two mNG molecules, see ***Methods***), suggesting it may have a dominant role in adhesion (***Figure 5A and B***). Loss of *ddr-2* resulted in a significant reduction in levels of both INA-1 and PAT-2 at the utse-seam BM-BM attachment through the L4 larval stage (***Figure 5B***). Taken together these data suggest DDR-2 could function to promote integrin adhesion within each tissue at the utse-seam connection.

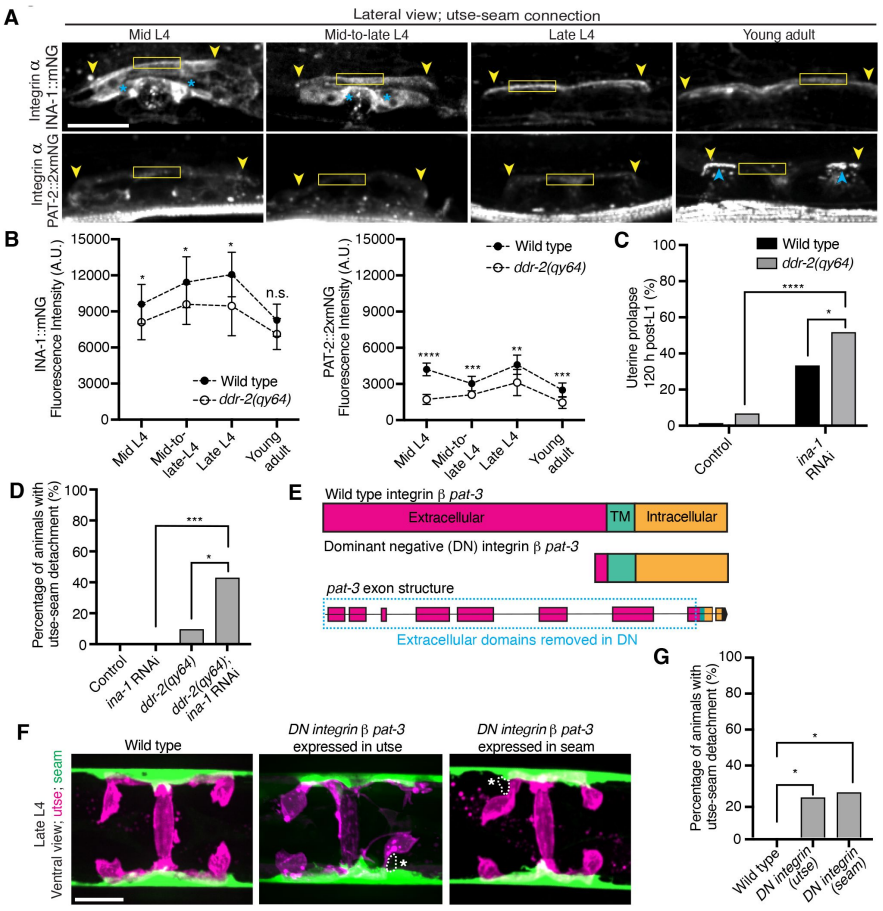

Figure 5 with 2 supplements

DDR-2 regulates integrin levels at the utse-seam connection and integrin functions in the utse and seam to mediate tissue attachment.

(A) Lateral fluorescence z-projections of integrin α subunits INA-1::mNG and PAT-2::2XmNG at the utse-seam connection (yellow arrowheads) from the mid L4 to young adult stages. Blue asterisks and arrowheads denote INA-1 signal in the developing vulva and PAT-2 at muscle attachment sites respectively. Fluorescence intensity at the utse-seam connection measured in yellow boxes. (**B**) Quantification of mean fluorescence intensity in wild-type and *ddr-2* knockout *(ddr-2(qy64))* animals (n ≥ 9 all conditions). Error bars represent SD. ****$P \leq 0.0001$, ***$P \leq 0.001$, **$P \leq 0.01$, *$P \leq 0.05$, n.s. (not significant), $P > 0.05$; unpaired two-tailed Student's *t* test. (**C**) Frequency of uterine prolapse in wild-type and *ddr-2(qy64)* animals treated with control or *ina-1* RNAi 120 h post-L1 plating. Control n = 1/70, *ddr-2(qy64)* n = 4/60, *ina-1* RNAi n = 22/66, and *ddr-2(qy64)*; *ina-1* RNAi n = 31/60 animals with uterine prolapse respectively. ****$P \leq 0.0001$, *$P \leq 0.05$; Fisher's exact test. (**D**) Frequency of utse-seam detachments in late L4 wild-type and *ddr-2(qy64)* animals treated with control or *ina-1* RNAi. Control n = 0/21, *ina-1* RNAi n = 0/25, *ddr-2(qy64)* n = 2/21, and *ddr-2(qy64)*; *ina-1* RNAi n = 9/21 animals with detachments respectively. ***$P \leq 0.001$, *$P \leq 0.05$; Fisher's exact test. (**E**) Schematic of dominant negative (DN) β integrin *pat-3*. (**F**) Ventral fluorescence z-projections of the utse *(cdh-3p::mCherry::PLC$^{\delta PH}$* or *nas-22p::2xmKate2::PLC$^{\delta PH}$)* and seam *(wrt-2p::GFP::PLC$^{\delta PH}$* or *scmp::GFP::CAAX)* cells in late L4 wild-type animals and animals expressing *DN integrin* in the utse (*zmp-1$^{mk50-51}$* promoter) or the seam (*wrt-2* promoter). Dotted lines with asterisks indicate regions of utse-seam detachment. (**G**) Percentage of animals with utse-seam detachment. Wild type, n = 0/19; *DN integrin (utse)*, n = 4/18; *DN integrin (seam)*, n = 4/16 animals with detachments respectively. *$P \leq 0.05$, Fisher's exact test. Scale bars, 20 μm.

Source data 1. Source data for ***Figure 5***. Raw data of INA-1/PAT-2 fluorescence intensity quantification used to generate ***Figure 5B*** in Microsoft Excel format. **Source data 2.** Source data for *Figure 5—figure supplement 1*. Raw data of fluorescence intensity quantification of matrix components and ZMP-4 at the utse-seam BM-BM linkage used to generate boxplots in *Figure 5—figure supplement 1* in Microsoft Excel format.

Source data 3. Source data for *Figure 5—figure supplement 2*. Raw data of fluorescence intensity quantification of *ina-1* knockdown used to generate plots in *Figure 5—figure supplement 2D and E* in Microsoft Excel format.

Figure supplement 1. *ddr-2* loss does not reduce functional levels of fibulin, hemicentin, type IV collagen, and matrix metalloproteinase ZMP-4 at the utse-seam connection; related to ***Figure 5***.

Figure supplement 2. The integrin α subunits INA-1 and PAT-2 are localized within both the utse and seam cells; related to ***Figure 5***.

We focused on a possible role for DDR-2 in regulating INA-1 at the utse-seam linkage, as INA-1 was present at higher levels compared to PAT-2 (***Figure 5A and B***) and was more enriched at cell surfaces (***Figure 5—figure supplement 2C***). Furthermore, PAT-2 anchors muscle attachments ((Moerman and Williams 2006), Gieseler, Qadota et al. 2017) (***Figure 5A***) and its loss leads to paralysis, which eliminates mechanical stress on the tissue connection and prevents defects in the utse-seam attachment (Gianakas, Keeley et al. 2023). To determine if DDR-2 promotes integrin activity, we reduced INA-1 levels at the late L4 stage to 30% by RNAi and assessed whether loss of *ddr-2* enhanced the Rup and utse-seam splitting defects (***Figure 5—figure supplement 2D and E***). Loss of *ddr-2* strongly enhanced the uterine prolapse defect caused by RNAi-mediated knockdown of *ina-1* (***Figure 5C***; ***Figure 5—figure supplement 2D***). In addition, loss of *ddr-2* enhanced the frequency of utse-seam detachments at the late L4 stage upon depletion of INA-1 (***Figure 5D***). We note that utse-seam detachments were not detected upon RNAi against *ina-1* alone, likely due to incomplete knockdown at this timepoint (***Figure 5—figure supplement 2D and E***). Together, these observations are consistent with a possible role for DDR-2 in regulating integrin function to promote utse-seam connection.

To determine where integrin functions to promote utse-seam attachment, we used a previously characterized dominant negative strategy, where expression of the β integrin PAT-3 lacking the extracellular domain (referred to as *DN integrin*; ***Figure 5E***) inhibits endogenous integrin function (Martin-Bermudo and Brown 1999; Hagedorn, Yashiro et al. 2009). We used the utse-specific *zmp-1*$^{mK50\text{-}51}$ promoter (***Figure 5—figure supplement 2F***) (Hagedorn, Yashiro et al. 2009) and the seam-specific *wrt-2* promoter to disrupt integrin activity in the respective tissues through the time of utse-seam tissue linkage (late L3 to young adult stages, ***Figure 1D***). Expression of *DN integrin* in either the utse or the seam cells resulted in utse-seam detachment at the late L4 (***Figure 5F and G***). Taken together, these findings indicate that DDR-2 may promote utse-seam BM-BM adhesion in part by regulating integrin levels and function.

DDR-2 promotes vinculin localization and integrin stability at the utse-seam linkage

As DDR-2 promotes integrin localization to the utse-seam BM-BM linkage and integrin activity promotes utse-seam attachment, we further explored how DDR-2 may regulate integrin. Talin and vinculin are core components of the integrin adhesion complex that support integrin activation (Chastney, Conway et al. 2021). We thus examined endogenously tagged talin (GFP::TLN-1) (Walser, Umbricht et al. 2017) and vinculin (DEB-1::mNG) localization and detected both proteins at the utse-seam attachment site. Levels of each protein ramped up to the late L4 and then decreased by the young adult stage, mirroring DDR-2 (***Figure 6A and B***). However, loss of *ddr-2* only decreased DEB-1 levels (***Figure 6B***). Confirming a role in utse-seam connection, depletion of DEB-1 by RNAi resulted in utse-seam detachment at the late L4 stage (***Figure 6C***; ***Figure 6—figure supplement 1***). These data show DDR-2 also regulates vinculin levels at the utse-seam linkage and that vinculin is required for utse-seam attachment. Integrin adhesions form stable complexes that anchor cells to ECM (Chastney, Conway et al. 2021). To determine whether DDR-2 regulates integrin complex stability at the site of utse-seam BM-BM tissue connection, we analyzed the dynamics of INA-1 by performing Fluorescence Recovery After Photobleaching (FRAP) experiments. We focused on INA-1::mNG at the late L4 stage when DDR-2 peaks in levels. Strikingly, loss of

ddr-2 nearly doubled the rate of recovery of INA-1::mNG fluorescence signal in the bleached region 10 minutes post-bleaching as compared to wild-type animals (***Figure 6D***). These observations indicate that DDR-2 stabilizes the INA-1 integrin adhesion complex at the utse-seam adhesion site.

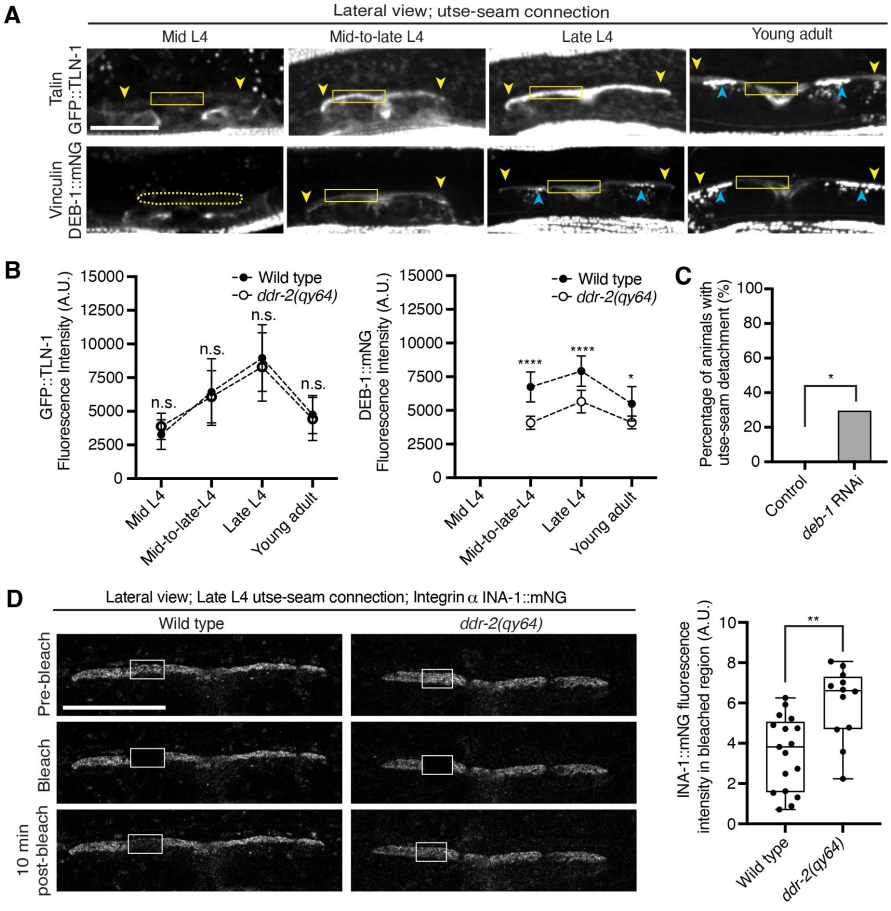

Figure 6 with 1 supplement

DDR-2 upregulates vinculin levels and stabilizes integrin at the utse-seam connection.

(**A**) Lateral fluorescence z-projections of the integrin activators talin (GFP::TLN-1) and vinculin (DEB-1::mNG) at the utse-seam attachment region (bounded by yellow arrowheads) from the mid L4 to young adult stages. Vinculin was not detected at the utse-seam attachment region at the mid L4 stage (dotted yellow box). Blue arrowheads indicate fluorescence signal at muscle attachment sites. Fluorescence intensity at the utse-seam attachment region was measured in the solid yellow boxes. (**B**) Quantification of TLN-1 and DEB-1 mean fluorescence intensity in wild-type and *ddr-2* knockout *(ddr-2(qy64))* animals (n ≥ 9 all conditions). Error bars represent SD. ****$P \leq 0.0001$, **$P \leq 0.01$, *$P \leq 0.05$, n.s. (not significant), $P > 0.05$; unpaired two-tailed Student's *t* test. (**C**) Frequency of utse-seam detachments observed in control or *deb-1* RNAi-treated late L4 animals. Control n = 0/21, *ina-1* RNAi n = 5/17 animals with detachments respectively. *$P \leq 0.05$, Fisher's exact test. (**D**) Left: Lateral fluorescence images of INA-1::mNG at the utse-seam connection before photobleaching, immediately after photobleaching, and 10 min post-photobleaching in late L4 wild-type and *ddr-2(qy64)* animals. Box indicates bleached region. Right: Quantification of mean INA-1::mNG fluorescence intensity in the bleached region 10 min post-photobleaching. Wild type, n = 17; *ddr-2(qy64)*, n = 12. **$P \leq 0.01$, unpaired two-tailed Student's *t* test. Scale bars, 20 µm. Box edges in boxplots represent the 25th and 75th percentiles, the line in the box denotes the median value, and whiskers mark the minimum and maximum values.

Source data 1. Source data for ***Figure 6***. Raw data of fluorescence intensity quantification of TLN-1 and DEB-1 as well as INA-1 recovery after photobleaching used to generate plots in ***Figure 6B and D*** in Microsoft Excel format.

Source data 2. Source data for ***Figure 6—figure supplement 1***. Raw data of fluorescence intensity quantification of *deb-1* knockdown at the utse-seam connection used to generate boxplot in ***Figure 6—figure supplement 1*** in Microsoft Excel format.

Figure supplement 1.*deb-1* knockdown efficiency; related to Figure 6C.

Ras acts in the DDR-2 pathway and promotes integrin adhesion at the utse-seam linkage

Vertebrate DDR2 activates multiple signaling networks, including the PI3K/Akt and Ras/Raf/Erk cascades (Payne and Huang 2014; Chen, Kong et al. 2021). Notably, Ras regulates integrin activity in several mammalian cell types (Zhang, Vuori et al. 1996; Conklin, Ada-Nguema et al. 2010; Sandri, Caccavari et al. 2012; Lilja, Zacharchenko et al. 2017). We thus hypothesized that DDR-2 could promote integrin stabilization through Ras signaling. We first strongly depleted LET-60 (see ***Methods***) the *C. elegans* Ras ortholog, and observed penetrant utse-seam attachment defects, which were not worsened in *ddr-2* null mutant animals (***Figure 7A***). This suggests that DDR-2 and LET-60/Ras function in the same pathway to mediate the utse-seam connection. Next, we analyzed INA-1::mNG levels and stability after LET-60 reduction. RNAi against *let-60* resulted in significantly lower INA-1 levels at the utse-seam BM-BM connection site (***Figure 7B***, pre-bleach panels and ***Figure 7—figure supplement 1***). Further, like loss of *ddr-2*, FRAP analysis indicated that depletion of LET-60/Ras reduced the stability of INA-1 at the utse-seam linkage site (*i.e.*, there was more rapid recovery of INA-1 after photobleaching (***Figure 7B***). We also generated animals harboring a gain-of-function mutation in Ras (LET-60^{G13E}, *let-60(qy203)*) (Singh and Han 1995). Strikingly, utse-seam detachments were observed in *let-60* gain-of-function animals (***Figure 7C***) and FRAP experiments revealed that INA-1 had an approximately two-fold greater stability at the utse-seam BM-BM connection site (***Figure 7D***). Collectively, these findings suggest that Ras acts downstream of DDR-2 to set the appropriate levels and stability of INA-1 mediated adhesion during the formation the utse-seam BM-BM tissue connection.

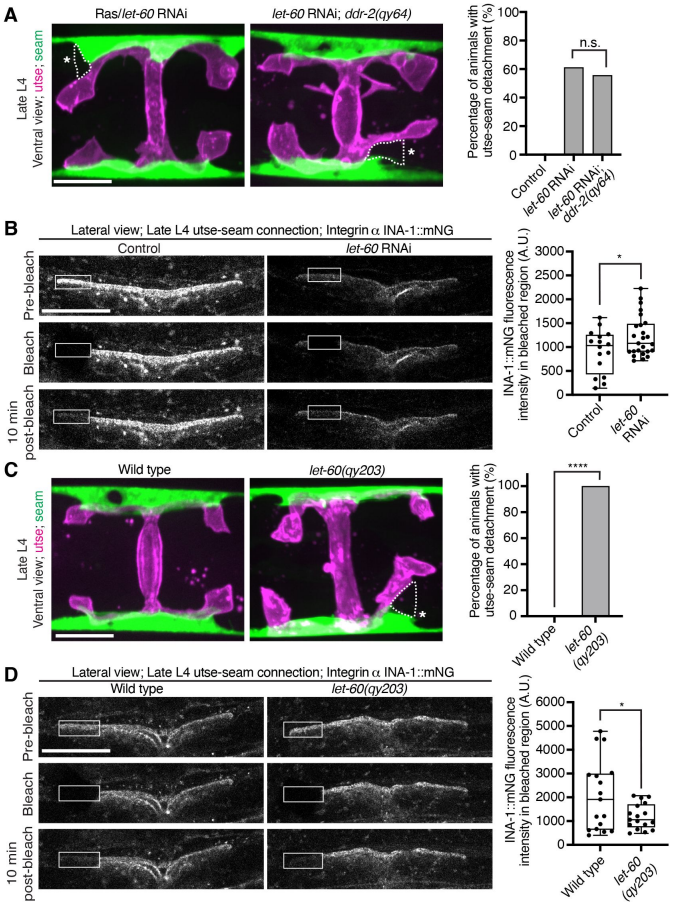

Figure 7 with 1 supplement

Ras/LET-60 acts in the same pathway as DDR-2 and controls integrin stability at the utse-seam tissue connection.

(A) Left: Ventral fluorescence z-projections of the utse *(nas-22p::2xmKate2::PLC$^{\delta PH}$)* and seam *(scmp::GFP::CAAX)* tissues in wild-type and *ddr-2* knockout *(ddr-2(qy64))* animals on Ras/*let-60* RNAi treatment. Dotted lines with asterisks indicate regions of utse-seam detachment. Right: Percentage of animals with utse-seam detachment. Control n = 0/21, *let-60* RNAi n = 11/18, and *let-60* RNAi; *ddr-2(qy64)*, n = 10/18 animals with detachments respectively. n.s. (not significant), $P > 0.05$; Fisher's exact test. (B) Left: Lateral fluorescence images of INA-1::mNG at the utse-seam connection before photobleaching, immediately after photobleaching, and 10 min post-photobleaching in late L4 control or *let-60* RNAi-treated animals. Box indicates bleached region. Right: Quantification of mean INA-1::mNG fluorescence intensity in the bleached region 10 min post-photobleaching. Control n = 16, *let-60* RNAi n = 25. *$P \leq 0.05$, unpaired two-tailed Student's *t* test. (C) Left: Ventral fluorescence z-projections of the utse and seam tissues in late L4 wild-type and *let-60* gain-of-function mutant *(let-60(qy203))* animals.

Dotted lines with asterisks indicate regions of utse-seam detachment. Right: Quantification of utse-seam detachment frequency. Wild type, n = 0/26; *let-60(qy203)*, n = 11/11 animals with detachments respectively. ****$P \leq 0.0001$, Fisher's exact test. (D) Left: Lateral fluorescence images of INA-1::mNG at the utse-seam attachment region before photobleaching, immediately after photobleaching, and 10 min post-photobleaching in late L4 wild-type and *let-60(qy203)* animals. Box indicates bleached region. Right: Quantification of mean INA-1::mNG fluorescence intensity in the bleached region 10 min post-photobleaching (n = 17 each genotype). *$P \leq 0.05$, unpaired two-tailed Student's *t* test. Scale bars, 20 µm. Box edges in boxplots represent the 25th and 75th percentiles, the line in the box denotes the median value, and whiskers mark the minimum and maximum values.

Source data 1. Source data for ***Figure 7***. Raw data of fluorescence intensity quantification of INA-1::mNG for photobleaching experiments used to generate boxplots in ***Figure 7B and D*** in Microsoft Excel format. Note that source data for ***Figure 7—figure supplement 1*** is found within ***Source data 1***.

Figure supplement 1. Ras/*let-60* knockdown reduces INA-1::mNG levels at the utse-seam connection; related to Figure 7B.

Discussion

To form organs such as the brain, kidney, and lung, separate tissues connect through adjoining basement membrane (BM) to mediate complex functions, such as molecular barrier, blood filtration, and gas exchange, respectively (Keeley and Sherwood 2019). These linkages resist the independent movement of each tissue and must be strong and balanced. How cells coordinate and strengthen adhesion at BM-BM linkage sites, however, is unknown. Using the *C. elegans* utse-seam BM-BM tissue connection, we show that type IV collagen, which is the molecular glue that fastens the BM-BM linkage, also activates the *C. elegans* collagen receptor DDR-2 in the utse and seam tissues. DDR-2 activity synchronizes and bolsters an integrin mediated adhesion to stabilize the utse-seam BM-BM tissue connection during its formation (***Figure 8***).

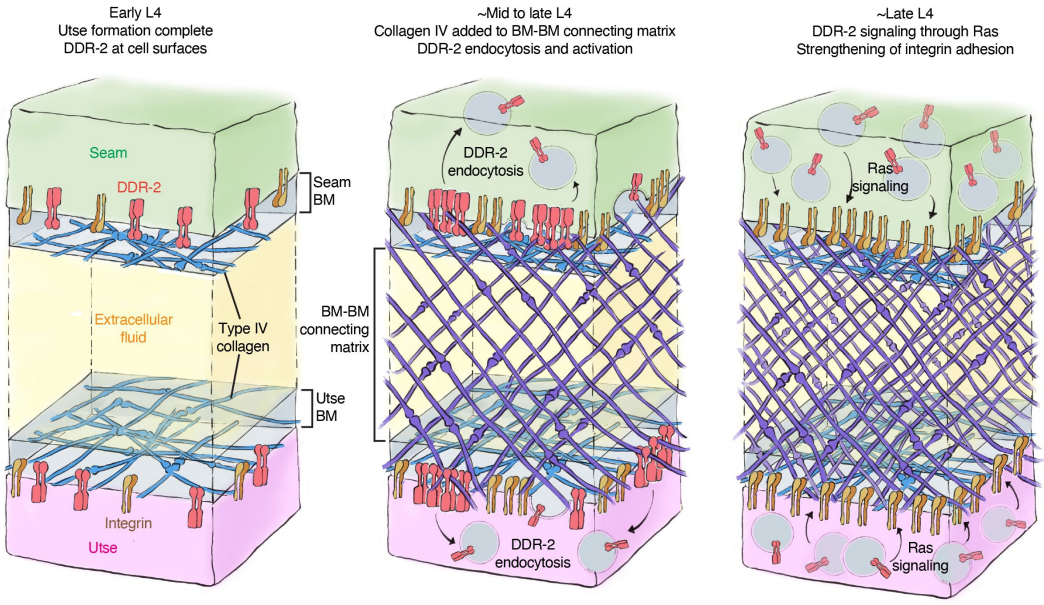

Figure 8

Model of DDR-2 function at the utse-seam tissue connection.

(A) At the early L4 larval stage, DDR-2 is predominantly found at the surfaces of utse and seam cells. (**B**) Between the mid and late L4 stages, type IV collagen assembles in the BM-BM connecting matrix to link the utse and seam tissues. Collagen addition and binding to DDR-2 triggers DDR-2 endocytosis and activation. (**C**) By the late L4, endocytic localization of DDR-2 reaches peak levels. Ras/LET-60 acts in the same pathway and may function downstream of DDR-2 to stabilize integrin adhesion. Thus, type IV collagen has a dual role in fastening the tissue connection and in signaling through DDR-2 to bolster cell adhesion at the linkage site.

The linkage between the multi-nucleated utse cell and epithelial seam cells allows the utse to maintain the uterus within the animal during powerful egg-laying muscle contractions (Vogel and Hedgecock 2001). We found that contact between the BM encased utse and seam cells occurs at the time the utse cell is formed during the early L4 larval stage. This association happens just prior to assembly of type IV collagen at the BM-BM linkage, a matrix component that allows the linkage to resist the mechanical forces of egg-laying (Gianakas, Keeley et al. 2023). Even before egg-laying, however, the utse-seam linkage resists the forces of body wall and uterine muscle contractions, as defects in matrix assembly linking the BMs results in utse-seam detachment during the mid L4 stage (Gianakas, Keeley et al. 2023). Through analysis of genetic mutations in the *C. elegans* receptor tyrosine kinase (RTK) DDR-2, an ortholog to the two vertebrate DDR receptors (DDR1 & DDR2) (Unsoeld, Park et al. 2013), we discovered that loss of *ddr-2* results in utse-seam detachment beginning at the mid L4 stage. The frequency of detachments in *ddr-2* mutant animals peaked around the late L4 stage and did not increase after this time. This correlated with the levels of DDR-2::mNG at the utse-seam connection, which peaked at the late L4 stage and then sharply declined by adulthood. Together, these findings suggest that DDR-2 promotes utse-seam attachment in the early formation of the tissue connection between the mid and late L4 stage. Analysis of the BM-BM connecting matrix that links the BMs, which is composed of hemicentin, fibulin-1, and type IV collagen, revealed it was still assembled at functional levels. This suggests that the utse and seam detachment did not arise from a reduction in

deposition of BM-BM linking matrix, but rather a defect in tissue adhesion to the BM-BM linkage site. Our results also indicated that DDR-2 functions in both the utse and seam to promote adhesion, as tissue specific expression of a dominant negative DDR-2 in either tissue resulted in utse-seam detachment. Loss of DDR1 in mice disrupts the BM-BM connection between the podocytes and endothelial cells in the kidney glomeruli and leads to defects in blood filtration (Gross, Beirowski et al. 2004), suggesting a possible shared function of DDR receptors in mediating proper linkage at sites of tissue connection.

In vitro studies using DDR-specific collagen binding peptides have revealed that DDRs only modestly contribute directly to cell adhesion (Xu, Bihan et al. 2012). Instead, DDRs are thought to initiate downstream signaling cascades that promote cell adhesion (Borza and Pozzi 2014). Consistent with this notion, we observed that DDR-2::mNG was not detectable at utse and seam cell surfaces when the *ddr-2* mutant attachment defect occurred between the mid to late L4 stages. Instead, DDR-2 was present in early, late, and recycling endosomes of both utse and seam cells. Work in a mouse osteoblast and a human kidney cell line has shown that DDR1 shifts from localization at the cell membrane to aggregation and internalization into early endosomes within minutes of exposure to collagen (Mihai, Chotani et al. 2009). Examination of the timing of DDR activation has suggested that full tyrosine receptor activation occurs within the endocytic vesicles (Mihai, Chotani et al. 2009; Murphy, Padilla et al. 2009; Villasenor, Kalaidzidis et al. 2016). We also found that internalization of DDR-2 at the utse-seam connection correlated with the assembly of type IV collagen at the BM-BM linkage and was dependent on type IV collagen deposition. Type IV collagen is ~400 nm in length and the utse-seam connecting matrix spans spans ~100 nm, while the utse and seam BMs are each ~50 nm thick (Timpl, Wiedemann et al. 1981; Vogel and Hedgecock 2001). Thus, collagen molecules in the connecting matrix could project into the utse and seam BMs to interact with DDR-2 on cell surfaces. Consistent with this possibility, super-resolution imaging of the mouse kidney glomerular basement membrane (GBM), a tissue connection between podocytes and endothelial cells, showed type IV collagen within the GBM projecting into the podocyte and endothelial BMs (Suleiman, Zhang et al. 2013; Naylor, Morais et al. 2021). As DDR-2 is activated by ligand-induced clustering of the receptor (Juskaite, Corcoran et al. 2017; Corcoran, Juskaite et al. 2019), it suggests that the BM-BM linking type IV collagen network, which is specifically assembled at high levels, clusters and activates DDR-2 in the utse and seam cells to coordinate cell-matrix adhesion at the tissue linkage site.

Vertebrate DDRs can promote integrin mediated cell-matrix adhesion in a variety of cell types. For example, overexpression of DDR1 enhances integrin matrix adhesion in human embryonic kidney cells and in human and mouse fibroblast (Xu, Bihan et al. 2012; Staudinger, Spano et al. 2013; Bayer, Grither et al. 2019). Several mechanisms for DDR-mediated enhancement of integrin adhesion have been proposed, including increased integrin surface levels and Rap1-mediated talin recruitment (Staudinger, Spano et al. 2013; Bayer, Grither et al. 2019). Loss of *C. elegans rap-1* has not been reported to have a Rup/uterine prolapse phenotype (Frische, Pellis-van Berkel et al. 2007) and we found that DDR-2 did not promote talin recruitment to the utse-seam connection. DDR-2 did, however, increase the levels of the two *C. elegans* α integrins—INA-1 and PAT-2—at the utse-seam linkage (Clay and Sherwood 2015), as well as the integrin activating protein DEB-1/vinculin (Bays and DeMali 2017). Supporting a functional role for DDR-2 in promoting INA-1 mediated utse-seam attachment, *ddr-2* null mutants strongly enhanced the utse-seam detachment and uterine prolapse defect (Rup phenotype) of animals with reduced INA-1 function. Further, like DDR-2, we found that INA-1 was expressed in the utse and seam cells and through tissue-specific expression of a dominant negative integrin, we determined that integrin activity is required in both tissues to promote adhesion. To understand how DDR-2 affects the strength of INA-1 mediated utse-seam adhesion, we performed photobleaching experiments on endogenously tagged INA-1::mNG, and discovered that DDR-2 stabilizes INA-1-mediated adhesion. Through genetic interaction studies, RNAi, and expression of constitutively active

Ras (*C. elegans* LET-60), we provide evidence that DDR-2 signals through Ras to promote INA-1 stability. Ras GTPases are a key downstream mediator of DDR signaling (Chen, Kong et al. 2021). Ras has been implicated in activating integrins via a poorly understood mechanism that may involve integrin receptor trafficking (Zhang, Vuori et al. 1996; Conklin, Ada-Nguema et al. 2010; Sandri, Caccavari et al. 2012). Interestingly, expression of the constitutively active form of Ras further increased INA-1 stability at the utse-seam linkage and led to a highly penetrant utse-seam detachment defect. Notably, our photobleaching experiments showed that there was a wide range of integrin stability at the utse-seam attachment site in wild-type animals, likely reflecting low to high adhesion strength. However, Ras activation narrowed integrin to within a high stability range (i.e. high adhesion strength), while *ddr-2* loss as well as Ras reduction shifted integrin towards a narrow, low stability range (low adhesion strength). Together, our observations suggest that DDR-2 signaling through Ras facilitates an increased range of integrin adhesion at the utse-seam connection, which is required to maintain the utse-seam linkage.

The utse-seam adhesion at the BM-BM tissue linkage is built in the L4 larval stage and then maintained in the adult to support egg-laying (Gianakas, Keeley et al. 2023). Our evidence indicates that DDR-2 activity is highest and perhaps only required between the mid and late L4 larval stages (~four-hour period), as the utse-seam detachment defect peaked by the mid-to-late L4 stage and did not worsen at the late L4 and young adult stages. This timing aligns with a spike in DDR-2 levels in the utse and seam cells and is also when DDR-2 most strongly promoted INA-1 integrin and vinculin levels at the utse-seam linkage. It is possible that DDR-2 is specifically required between the mid and late L4 stages to facilitate a wide range of integrin adhesion. This could adjust the cell-matrix adhesion strength as the BM-BM connecting matrix assembles, strengthens, and changes composition during this time window, shifting from a hemicentin and fibulin-rich to a type IV collagen-dominated matrix (Gianakas, Keeley et al. 2023). Alternatively, a range of integrin adhesion strength may be required to maintain the utse-seam linkage, while allowing the utse and seam to undergo morphogenetic changes to form the tongue (utse) and groove (seam) morphology that secures the tissue linkage. Collectively, our findings support the idea that although the ligands for DDRs are stable collagen molecules, DDRs can function as dynamic sensors of the external environment, allowing cells and tissues to coordinate their activities with changes to the extracellular surroundings.

Materials and Methods

Key resources table

Reagent type (species) or resource	Designation	Source or reference	Identifiers	Additional information
Strain, strain background (*C. elegans*)	NK2617	(Gianakas, Keeley et al. 2023)		*qyIs23 [cdh-3p::mCh::PH]* II*; lqIs80 [scmp::GFP::CAAX]* IV
Strain, strain background (*C. elegans*)	N2	Caenorhabditis Genetics Center (CGC)		Wild type (ancestral)
Strain, strain background (*C. elegans*)	RB970			*ddr-1(ok874)* X
Strain, strain background (*C. elegans*)	VH1387	(Unsoeld, Park et al. 2013)		*ddr-1(tm382)* X
Strain, strain background (*C. elegans*)	RB788			*ddr-2(ok574)* X
Strain, strain background (*C. elegans*)	VH1383	(Unsoeld, Park et al. 2013)		*ddr-2(tm797)* X

Strain, strain background (*C. elegans*)	NK2511	This study		*ddr-2(qy64)* X
Strain, strain background (*C. elegans*)	NK2655	This study		*qyIs23 [cdh-3p::mCh::PH]* II; *lqIs80 [scmp::GFP::CAAX]* IV; *ddr-2(qy64)* X
Strain, strain background (*C. elegans*)	NK2640	This study		*qy91 [nas-22p::2xmKate2::PH*] II; *lqIs80* [*scmp::GFP::CAAX*] IV
Strain, strain background (*C. elegans*)	NK2682	This study		*qy91 [nas-22p::2xmKate2::PH]* II; *lqIs80 [scmp::GFP::CAAX]* IV; *ddr-2(qy64)* X
Strain, strain background (*C. elegans*)		This study		*qy44 [ddr-2::mNG]* X; *qyEx605 [scmp::2xmKate2:PH]*

Strain, strain background (*C. elegans*)	NK2620	This study		*qyIs23 [cdh-3p::mCh::PH]* II; *qy44 [ddr-2::mNG]* X
Strain, strain background (*C. elegans*)	NK2763	This study		*qyIs256 [cdh-3p::mCherry::rab-5]* ?; *qy44 [ddr-2::mNG*] X
Strain, strain background (*C. elegans*)	NK2766	This study		*qyIs252 [cdh-3p::mCherry::rab-7]* ?; *qy44 [ddr-2::mNG*] X
Strain, strain background (*C. elegans*)	NK2769	This study		*qyIs205 [cdh-3p::mCherry::rab-11]* ?; *qy44 [ddr-2::mNG*] X
Strain, strain background (*C. elegans*)	NK2901	This study		*qy188 [scmp::mKate2::rab-5]* I; *qy44 [ddr-2::mNG*] X
Strain, strain background (*C. elegans*)	NK2926	This study		*qy91 [nas-22p::2xmKate2::PH*] II; *IqIs80* [*scmp::GFP::CAAX*] IV; *ddr-2(ok574)* X

Strain, strain background (*C. elegans*)	NK2705	(Jayadev, Morais et al. 2022)		*qy118 [col-99::mNG (internal tag)]* IV
Strain, strain background (*C. elegans*)	NK2322	(Keeley, Hastie et al. 2020)		*qy22 [cle-1::mNG]* I
Strain, strain background (*C. elegans*)	NK2326	(Keeley, Hastie et al. 2020)		*qy24 [emb-9::mNG (internal tag)]* III
Strain, strain background (*C. elegans*)	NK2830	This study		*qy166 [cdh-3p::dominant negative ddr-2::mNG]* I; *qy91 [nas-22p::2xmKate2::PH]* II; *heIs63 [wrt-2p::GFP::PH + wrt-2p::GFP::H2B + lin-48p:mCherry]* V
Strain, strain background (*C. elegans*)	NK2848	This study		*qy175 [scmp::dominant negative ddr-2::mKate2]* I; *qy91 [nas-22p::2xmKate2::PH]*

				II; *heIs63 [wrt-2p::GFP::PH + wrt-2p::GFP::H2B + lin-48p:mCherry]* V
Strain, strain background (*C. elegans*)	NK2585	(Jayadev, Morais et al. 2022)		*qy83 [emb-9::mRuby2 (internal tag)]* III
Strain, strain background (*C. elegans*)	NK2422	(Keeley, Hastie et al. 2020)		*qy33 [him-4::mNG]* X
Strain, strain background (*C. elegans*)	NK2324	(Jayadev, Chi et al. 2019)		*qy23 [ina-1::mNG]* III
Strain, strain background (*C. elegans*)	NK2479	(Jayadev, Chi et al. 2019)		*qy49 [pat-2::2xmNG]* III
Strain, strain background (*C. elegans*)	NK2825	This study		*qy23 [ina-1::mNG]* III; *ddr-2(qy64)* X
Strain, strain background (*C. elegans*)	NK2858	This study		*qy49 [pat-2::2xmNG]* III; *ddr-2(qy64)* X
Strain, strain background (*C. elegans*)	NK2804	This study		*qyIs23 [cdh-3p::mCh::PH]* II; *heIs63 [wrt-*

				2p::GFP::PH + wrt-2p::GFP::H2B + lin-48p:mCherry] V
Strain, strain background (*C. elegans*)	NK2824	This study		*qyIs23 [cdh-3p::mCh::PH]* II; *qyIs15 [zmp-1$^{mk50-51}$p::dominant negative integrin b-pat-3]* IV;*heIs63 [wrt-2p::GFP::PH + wrt-2p::GFP::H2B + lin-48p:mCherry]* V
Strain, strain background (*C. elegans*)	NK2934	This study		*qy91 [nas-22p::2xmKate2::PH]* II; *unc-119(ed4)* III; *lqIs80* [*scmp::GFP::CAAX*] IV; *qyEx604 [wrt-2p::dominant negative integrin b-pat-3 + unc-119(+)]*
Strain, strain background (*C. elegans*)	NK2579	(Keeley, Hastie et al. 2020)		*qy62 [mNG::fbl-1] IV*

Strain, strain background (*C. elegans*)	NK932	(Kelley, Chi et al. 2019)		*qyIs190 [zmp-4p::zmp-4::GFP]*
Strain, strain background (*C. elegans*)	NK268	(Hagedorn, Yashiro et al. 2009)		*qyIs17 [zmp-1$^{mk50-51}$p mCherry]*
Strain, strain background (*C. elegans*)	AH3437	(Walser, Umbricht et al. 2017)		*zh117 [GFP::tln-1]* I
Strain, strain background (*C. elegans*)	NK2478	This study		*qy48 [deb-1::mNG]* IV
Strain, strain background (*C. elegans*)	NK2854	This study		*zh117 [GFP::tln-1]* I; *ddr-2(qy64)* X
Strain, strain background (*C. elegans*)	NK2860	This study		*qy48 [deb-1::mNG]* IV; *ddr-2(qy64)* X
Strain, strain background (*C. elegans*)	NK2944	This study		*qy91 [nas-22p::2xmKate2::PH]* II; *lqIs80* [*scmp::GFP::CAAX*] IV; *let-60(qy203)* IV

Strain, strain background (*C. elegans*)	NK2957	This study		*qy23 [ina-1::mNG]* III; *let-60(qy203)* IV
Strain, strain background (*E. coli*)	*emb-9* RNAi	(Kamath and Ahringer 2003)		Clone from Ahringer library (L4440 vector backbone)
Strain, strain background (*E. coli*)	*col-99* RNAi	(Rual, Ceron et al. 2004)		Clone from Vidal library (L4440 vector backbone)
Strain, strain background (*E. coli*)	*cle-1* RNAi	(Rual, Ceron et al. 2004)		Clone from Vidal library (L4440 vector backbone)
Strain, strain background (*E. coli*)	*ina-1* RNAi	(Rual, Ceron et al. 2004)		Clone from Vidal library (L4440 vector backbone)
Strain, strain background (*E. coli*)	*let-60* RNAi	(Rual, Ceron et al. 2004)		Clone from Vidal library (L4440 vector backbone)
Strain, strain background (*E. coli*)	*deb-1* RNAi	(Rual, Ceron et al. 2004)		Clone from Vidal library (L4440 vector backbone)
Strain, strain background (*E. coli*)	*him-4* RNAi	(Gianakas, Keeley et al. 2023)		T444t vector backbone

Strain, strain background (*E. coli*)	*ddr-2* RNAi	This study		T444t vector backbone
Sequence-based reagent	*ddr-2* knockout (*ddr-2(qy64)*) sgRNA 1	This study		ATCCTGACATAGA TGAGCGT
Sequence-based reagent	*ddr-2* knockout (*ddr-2(qy64)*) sgRNA 2	This study		GTCATTGGTGCAC ACTTCTC
Sequence-based reagent	*ddr-2* knockout (*ddr-2(qy64)*) sgRNA 3	This study		AAGTGTGCACCAA TGACTGG
Sequence-based reagent	*deb-1::mNG* (*deb-1(qy48)*) sgRNA 1	This study		AGTTGGACCACAT TGGCTTT
Sequence-based reagent	*deb-1::mNG* (*deb-1(qy48)*) sgRNA 2	This study		ATTTAGAAGTTGG ACCACAT
Sequence-based reagent	*let-60* gain-of-function (*let-60(qy203)*) sgRNA 1	This study		CTTGTGGTAGTTG GAGATGG
Sequence-based reagent	Primer *ddr-2(qy64)* homology arm forward	This study		TTTTCAGAGTCTC CGACGCTCATCTA

Sequence-based reagent	Primer *ddr-2(qy64)* homology arm reverse	This study		TAAATATTATTCTGAGAATATA
Sequence-based reagent	Primer *ddr-2(qy64)* genotyping forward	This study		TGGTAATTGATGAGAGGGTG
Sequence-based reagent	Primer *ddr-2(qy64)* genotyping reverse	This study		TGTCGTTTCGACACCGGCAA 1.8 kb band
	Primer *let-60(qy203)* homology arm forward	This study		ATGACGGAGTACAAGCTTGTGGTAGTTGGAGATGGAGAAGT
	Primer *let-60(qy203)* homology arm reverse	This study		TACCCTTTTCTGAAAAAGACGC
Sequence-based reagent	Primer *nas-22* promoter forward	This study		TCAAAGCGTCAAGCTTTACG

Sequence-based reagent	Primer *nas-22* promoter reverse	This study		TTTTCTGTCTACAAGGACTGTGC
Sequence-based reagent	Primer *scm* promoter forward	(Chapman, Li et al. 2008)		AACCTCCACCAGATGGTTGGCG
Sequence-based reagent	Primer *scm* promoter reverse	(Chapman, Li et al. 2008)		CCCGGGGATCCGTCCACTCT
Sequence-based reagent	Primer *cdh-3* promoter forward	This study		CTAGAGCATGATGTCCTTAC
Sequence-based reagent	Primer *cdh-3* promoter reverse	This study		CAAAACGGACCGACCGTCCC
Sequence-based reagent	Primer *dominant negative ddr-2* forward	This study		ATGAAGTTGCTGCTGTATCT
Sequence-based reagent	Primer *dominant negative ddr-2* reverse	This study		TCTGCTCACGCAAATCAACT

Sequence-based reagent	Primer *wrt-2* promoter forward	This study		TCAGAACTCTAATACTTACT
Sequence-based reagent	Primer *wrt-2* promoter reverse	This study		CCGAGAAACAATTGGCAGGT
Sequence-based reagent	Primer *dominant negative integrin b pat-3* forward	(Hagedorn, Yashiro et al. 2009)		TCTAGAGGATCCCGGGGAT
Sequence-based reagent	Primer *dominant negative integrin b pat-3* reverse	(Hagedorn, Yashiro et al. 2009)		ATTTAGTTGGCTTTTCCAGC
Sequence-based reagent	Primer *ddr-2* RNAi forward	This study		ATGAAGTTGCTGCTGTATCT
Sequence-based reagent	Primer *ddr-2* RNAi reverse	This study		ATGAATATGAGGAGAAGTGTGC
Recombinant DNA reagent	Plasmid: pCFJ352	Addgene	RRID: Addgene_30539	sgRNA targeting MosSCI insertion

				site on Chr I, from Erik Jorgensen
Recombinant DNA reagent	Plasmid: pDD122	(Dickinson, Ward et al. 2013)	RRID: Addgene_47550	sgRNA targeting MosSCI insertion site on Chr II
	Plasmid: pAP087	(Pani and Goldstein 2018)		starter SEC repair template plasmid for single copy insertion at the ttTi5605 site on chromosome II
Recombinant DNA reagent	Plasmid: pAP088	(Pani and Goldstein 2018)		starter SEC repair template plasmid for single copy insertion at the ttTi4348 site on chromosome I
Chemical compound, drug	Ampicillin	Sigma-Aldrich	#A0166	
Chemical compound, drug	Isopropyl β-D-1-thiogalactopyranoside	Sigma-Aldrich	#I6758	
Chemical compound, drug	Hygromycin B	Sigma-Aldrich	#H3274	
Chemical compound, drug	Sodium azide	Sigma-Aldrich	#S2002	

Chemical compound, drug	Levamisole	Sigma-Aldrich	#L9756	
Software, algorithm	µManager v.1.4.23			
Software, algorithm	Zen Black			
Software, algorithm	Fiji/ImageJ			
Software, algorithm	GraphPad Prism v9			

C. elegans culture and strains

C. elegans strains used in this study are listed in the ***Key resources table***. Worms were reared on nematode growth medium plates seeded with OP50 *Escherichia coli* at 16°C, 18°C, or 20°C according to standard procedures (Stiernagle 2006). We used *C. elegans* vulval development to accurately stage animals through the morphogenesis of the utse-seam connection (late L3 to young adult stage) (Mok, Sternberg et al. 2015).

Generation of genome-edited strains

To generate the genome-edited mNeonGreen (mNG) knock-in allele for *deb-1* (*qy48*), we used CRISPR/Cas9 genome editing with a self-excising cassette (SEC) for drug selection (hygromycin treatment) as described previously (Dickinson, Ward et al. 2013; Keeley, Hastie et al. 2020). An 18 amino acid flexible linker attached to the mNG fluorophore was inserted in frame and directly upstream of the stop codon. sgRNA sequences directing Cas9 cleavage near the C-terminus are provided in the ***Key resources table***.

The *ddr-2* knockout allele *ddr-2(qy64)*, an 8615 bp deletion corresponding to the coding sequence of DDR-2, was also generated with the SEC CRISPR method detailed above with one modification—we generated a new starter repair plasmid lacking the fluorescent tag. Primers used to amplify homology arms, sgRNA sequences to direct Cas9 cleavage, and genotyping primers used to verify genome-edited knockout animals are provided in the ***Key resources table***.

For the LET-60^{G13E} gain-of function mutation, *let-60(qy203)*, we used the same strategy as the *ddr-2* knockout allele. The point mutation was incorporated into the primer for homology arm amplification. Note that this mutation is identical to the *let-60(n1046)* allele.

Generation of transgenic strains

For the utse marker *qy91 [nas-22p::2xmKate2::pH]*, we generated a single-copy transgene inserted into the ttTi5605 transposon insertion on chromosome II (Frokjaer-Jensen, Davis et al. 2012) using the SEC CRISPR method detailed above. A 2 kb *nas-22* promoter, two tandem mKate2 fluorophores attached to a PH domain, and an *unc-54* 3' UTR fragment were ligated in order via Gibson assembly into the pAP087 starter repair plasmid containing homology arms for the ttTi5605 site. The sgRNA directing Cas9 cleavage near this region is contained in the pDD122 vector.

To express mKate2-tagged RAB-5 in the seam, we generated a single-copy transgene inserted into the ttTi4348 transposon insertion site on chromosome I (Frokjaer-Jensen, Davis et al. 2012) using SEC CRISPR. Briefly, the scm promoter, mKate2 fluorophore, rab-5 genomic sequence, and *unc-54* 3' UTR were Gibson assembled in order into the pAP088 starter repair plasmid containing homology arms for the ttTi4348 site. The sgRNA directing Cas9 cleavage near this region is contained in the pCFJ352 vector.

For tissue-specific expression of dominant negative (DN) DDR-2 in the utse or seam, we also generated single-copy transgenes inserted into the ttTi4348 site. For utse expression, the following fragments were Gibson assembled in order into pAP088: a 1.5kb *cdh-3* promoter fragment, *DN ddr-2*, mNG fluorophore, and *unc-54* 3' UTR. Expression in transgenic animals was verified by assessing mNG fluorescence. For seam expression, the following fragments were Gibson assembled in order into pAP088: the *scm* promoter fragment, *DN ddr-2*, and mKate2 fluorophore. Expression in transgenic animals was verified by assessing mKate2 fluorescence.

The seam cell marker *qyEx605 [scmp::2xmKate2::PH]* was built by Gibson assembling a 1.3 kb *scm* promoter fragment, a fragment with two tandem mKate2 fluorophores attached to the PH domain, and *unc-54* 3' UTR fragment in order. The construct was expressed as extrachromosomal arrays as described previously (Yochem and Herman 2003).

To build the construct for *DN integrin* expressed in the seam, we first amplified the *DN integrin* fragment from animals harboring the *qyIs15* allele (see ***Key resources table***). The *DN integrin* fragment is composed of a *pes-10* enhancer element, the *ost-1* signal peptide, the *pat-3* β-tail fragment, and *unc-54* 3' UTR as described previously (Lee Cram et al. 2001). The *DN integrin* fragment was fused to a 1.3 kb *wrt-2* promoter by PCR. The construct was expressed extrachromosomally.

RNAi

All RNAi constructs except for *ddr-2* RNAi were obtained from the Ahringer and Vidal RNAi libraries (Kamath and Ahringer 2003; Rual, Ceron et al. 2004) or generated previously (Gianakas, Keeley et al. 2023). For the *ddr-2* clone, a ~2.4 kb cDNA fragment corresponding to the longest *ddr-2* transcript was amplified by PCR and inserted into the T444t vector as described previously (Gianakas et al 2023). RNAi experiments were performed using the feeding method (Timmons, Court et al. 2001) according to previously detailed protocols (Jayadev, Chi et al. 2019; Gianakas, Keeley et al. 2023). For experiments assessing the utse-seam connection, RNAi was initiated in synchronized L1 larvae and animals were examined at the late L4 stage (~ 44 h treatment). For examination of uterine prolapse, RNAi was performed from the L1 through adulthood (~ 120 h treatment). For depletion of hemicentin initiated at the early L4 stage, synchronized L1 worm were grown on control RNAi for ~ 38 h to the early L4, and then transferred onto *him-4* RNAi to the late L4 (~5-6 h treatment). We verified knockdown efficiencies for all RNAi experiments except for *let-60* RNAi by including a control with the relevant fluorescent tagged target protein, achieving between ~75 to 100% reduction. We verified *let-60* RNAi knockdown efficiency by plate level assessment of brood size, which was strongly reduced compared to control animals, as previously reported (Ceron, Rual et al. 2007).

Microscopy and image processing

All fluorescence images (except for photobleaching experiments) were acquired at 20°C on Zeiss Axio Imager A1 microscopes controlled by the μManager software v.1.4.23 or v.2.0.1 (Edelstein, Amodaj et al. 2010), equipped with a Hamamatsu ImagEM electron multiplying

charge-coupled device camera or an Orca-Fusion scientific complementary metal oxide semiconductor camera, Zeiss 40x and 100x Plan Apochromat (1.4 numerical aperture) oil immersion objectives, Yokogawa CSU-10 spinning disc confocal scan heads, and 488 nm, 505 nm, and 561 nm laser lines. Worms were mounted on 5% noble agar pads containing 0.01M sodium azide for imaging.

For photobleaching experiments, images were acquired at 20°C on a Zeiss 880 single-point scanning confocal attached to a Zeiss Axio Observer Z1 microscope, with a Marzhauser linearly encoded stage, a 40x Plan Neofluar (1.3 numerical aperture) oil immersion objective, and a 488 nm laser line. Worms were anesthetized by soaking in 5 mM levamisole in M9 buffer for 15 min and then transferred to 4% noble agar pads. Coverslips were then placed and sealed on top with valap (equal weight Vaseline, lanolin, and paraffin) and flooded with 5 mM levamisole. Coverslip sealing kept the animals hydrated during the experimental timeframe, ensuring accurate imaging of endogenous protein dynamics (detailed in (Kelley, Wang et al. 2017)). A rectangle region within one arm of the BM-BM connection BLINK was photobleached using 30 iterations of simultaneous 405 nm and 488 nm excitation at 100% laser power for a total bleaching time of 1.5 seconds. Worms were imaged prior and immediately following bleaching, and then again 10 min later.

Brightfield images of worms were acquired at 20°C on a Zeiss Axio Zoom V16 stereo fluorescence microscope controlled by Zen 3.2 software, equipped with an Axiocam digital camera and a 3x objective. Worms were imaged without immobilization.

To image the utse and seam cells ventrally, we manually oriented animals in the ventral orientation (Kelley, Wang et al. 2017) and acquired z-stacks at 0.37 µm intervals, capturing the entire H-shaped structure of the utse and the seam cells flanking both sides of the utse at 100x magnification. Ventral views of the utse and seam shown in figures are maximum intensity projections of these z-stacks. 3D isosurface renderings of the utse and seam cells shown in ***Figure 2D*** were generated with Imaris 7.4 software (Bitplane). We acquired lateral z-stacks at 0.37 µm intervals to fully capture the superficial half of the utse-seam attachment.

For lateral imaging of DDR-2::mNG together with the utse, seam cells, or endosome markers expressed in the utse or seam, we acquired z-stacks at 0.37 µm intervals to capture as much of each tissue that was in focus superficially at 40x magnification. Images shown in figures are single slices where DDR-2 was sharply in focus within the tissue of interest. The same parameters were used for imaging INA-1::mNG and PAT-2::mNG in the utse and seam. Images in ***Figure 5A*** correspond to the z-slices where INA-1 and PAT-2 were most in focus at the BM-BM connection region. In ***Figure 5—figure supplement 2A and B***, images shown are sum projections of the seam or utse regions.

To image DDR-2::mNG specifically at the utse-seam attachment site, we acquired lateral z-stacks at 0.37 µm intervals capturing both the surface of the utse and the seam cells. We used a utse cell marker as a reference to accurately capture this region (see also schematic in ***Figure 3A***). Images shown in ***Figure 4*** are sum projections of these z-stacks.

For lateral imaging of respective tagged proteins at the BM-BM connection region, we acquired single slices (40x magnification) at the middle focal plane where the BM-BM connection signal was sharply in focus. All images were process in Fiji 2.0 (Schindelin, Arganda-Carreras et al. 2012).

Image analysis and quantification

To assess utse-seam detachment, we used maximum intensity projections of the utse and seam viewed ventrally as detailed above. We defined utse-seam detachment as any gap in the utse-seam attachment of at least 4 square pixels in area. We preferred the ventral view

over 3D rendering for this metric as gaps were variable in size and location (typically occurring in one or two arms of the utse on opposite sides). The ventral projections allowed us to reliably examine all four arms of the utse and whether they were in contact with the seam from animal to animal. The visual representation of a gap in a ventral maximum projection is an underestimate of the true size of the detachment, as the tongue-in-groove association of the utse and seam can only be seen in a 3D surface rendering of the utse and seam viewed from the side. We thus used a binary scoring system (animals with or without utse-seam detachments) instead of quantifying the size of the detached region. We note that ventral imaging of the utse and seam sometimes results in small utse-seam detachments as we manually orient the animals on the slide. To control for this, we acquired large datasets (at least 40 animals examined) for every control strain we used to visualize the utse-seam attachment with. We found that small detachments related to ventral imaging occurred in ~8-12% of animals, depending on the genetic background. All datasets shown in figures have been normalized to account for this.

All quantifications of mean fluorescence intensity were done on raw images in Fiji 2.0. We drew ~5-pixel long and 2-pixel wide linescans to obtain raw values of mean fluorescence intensity. We measured mean fluorescence intensity for all quantifications in order to account for linescan area. For measurement within the BM-BM connection region, we positioned the linescan within the arm that was most in focus. Other regions where linescans were performed are indicated in figures. Background intensity values were obtained with similar linescans in adjacent regions with no visible fluorescence signal. Note that we used two tandem mNG fluorophores to visualize PAT-2 at the utse-seam attachment site (PAT-2::2xmNG) as it was present at very low levels. We imaged PAT-2::mNG and PAT-2::2xmNG in this region at the same exposure and found that the latter was approximately two times brighter (PAT-2::2xmNG mean fluorescence intensity 3941 ± 847 A.U., PAT-2::mNG 2037 ± 465 A.U., n = 10 animals examined each). Taken together with quantifications in ***Figure 5B***, INA-1 is thus likely present at six-fold higher levels than PAT-2 at the utse-seam attachment site. For additional quantification related to FRAP, see below.

For FRAP analysis, we measured mean fluorescence intensity within the bleached region. In addition, we performed an equivalent linescan within the unbleached arm at the BM-BM connection to calculate a bleach correction factor to account for general photobleaching during image acquisition across the duration of the experiment, as previously described (Gianakas, Keeley et al. 2023). Briefly, the background-corrected fluorescence intensity measurement on the side of the BM-BM connection where FRAP was not performed at the 10 min post-bleach timepoint was divided by the respective value at the pre-bleach timepoint to obtain the bleach correction factor. Fluorescence intensity measurements at the pre-bleach and post-bleach timepoints on the side of the BM-BM connection where FRAP was performed were then multiplied by the respective bleach correction factor to normalize these values to the 10 min post-bleach fluorescence intensity measurement in the same region.

To count the number of DDR-2 punctae at the site of utse-seam attachment, we used sum projections of DDR-2::mNG capturing the surface of the utse and seam (described earlier). We restricted measurements to the utse-seam connection corresponding to one utse arm. Brightness and contrast was then adjusted to manually count individual punctae, as DDR-2 punctae showed a large variance in size and fluorescence intensity. Note that in the type IV collagen depletion condition, we only counted discrete puncta and did not include the large cell surface accumulation of DDR-2 in the analysis.

To determine co-localization of DDR-2 with markers of endocytic vesicles, we also used a manual approach due to the large variability of the size and fluorescence intensity of punctae. We selected a single slice where the utse or the seam was sharply in focus, and restricted measurements to a single utse arm or a region of the seam corresponding to a

single utse arm. For each animal, the number, and positions of DDR-2 punctae were noted and compared to the respective endosome marker (RAB-5, RAB-7, or RAB-11). If a DDR-2 puncta physically overlapped with or was in contact with an endosome punctum, it was classified as one that co-localized with the endosomal marker. We then calculated the percentage overlap of DDR-2 punctae with the vesicle marker for each animal (corresponding to each data point within boxplots in ***Figure 3—figure supplement 1B and C***).

Scoring of uterine prolapse

Uterine prolapse frequency was assessed as described previously (Gianakas, Keeley et al. 2023). Briefly, synchronized L1 larvae were plated (~20 animals per plate) and after 24 h, the exact number of worms on each plate was recorded. Plates were then visually screened for ruptured worms (uterine prolapse) every 24 h during egg-laying (between 48 h to 120 h post-L1). We chose to examine the entire egg-laying period as ruptures arising from utse-seam detachments do not usually occur at the onset of egg-laying, but after cycles of egg-laying that place repeated mechanical stress on the utse-seam connection (Gianakas, Keeley et al. 2023). Ruptured animals were scored and removed from plates to avoid double counting and after 120 h, the percentage of animals with uterine prolapse was calculated. At least 50 animals were screened for every experiment.

Illustrations of utse-seam tissue connection

For schematics in Figure 1A and Figure 8, model protein sizing was scaled according to previously generated models (Keeley, Hastie et al. 2020). We sized hemicentin, fibulin, type IV collagen, integrin, and DDR-2. We also approximated the span of the basement membranes of the utse and seam cells (~50 nm each), as well as the BM-BM connecting matrix (~200 nm), based on electron microscopy of the utse-seam attachment (Vogel and Hedgecock 2001).

Statistical analysis

Statistical analysis was performed in GraphPad Prism 9. Normality of datasets was assessed using the D'Agostino-Pearson normality test. We used parametric tests for datasets that followed a Gaussian distribution and non-parametric tests for those that did not. For comparisons of means between two populations, we used either an unpaired two-tailed Student's *t* test or a Mann-Whitney *U* test. For comparisons of means between three or more populations, we performed either a one-way ANOVA followed by post hoc Dunnett's test or Kruskal-Wallis *H* test with post hoc Dunn's test. For comparisons between two categorical variables, we used the Fisher's exact test. All graphs were prepared in GraphPad Prism. Figure legends indicate sample sizes, statistical tests used, and *P* values.

Data availability

All data generated in this study are included in the manuscript and supporting files.

Acknowledgements

We would like to thank C. Borza, A. Pozzi, B. Hoffman, and D. Reiner for helpful discussions, C. Gianakas for comments on the manuscript, and M. Boxem and H. Hutter for strains. Some

strains were provided by the CGC, which is funded by NIH Office of Research Infrastructure Programs (P40 OD010440). S.G.P. was supported by graduate research fellowship NICHD F31 HD97901. This work was supported by R35GM118049, R21OD028766, and R21OD032430 to D.R.S.

Additional Information

Funding

Funder	Grant reference number	Author
National Institutes of Health	R35GM118049	David R. Sherwood
National Institutes of Health	R21OD028766	David R. Sherwood
National Institutes of Health	R21OD032430	David R. Sherwood
National Institute of Child Health and Human Development	F31 HD97901	Sara G. Payne

Author Contributions

Kieop Park, conceptualization, data curation, formal analysis, investigation, visualization, methodology, writing-original draft; Ranjay Jayadev, conceptualization, data curation, formal analysis, investigation, visualization, methodology, writing-original draft; Sara G. Payne, Conceptualization, data curation, formal analysis, investigation, visualization, methodology, writing-original draft, funding acquisition; Isabel W. Kenny-Ganzert, investigation, methodology; Qiuyi Chi, investigation, methodology; Daniel S. Costa, methodology; William Ramos-Lewis, investigation, methodology; Siddharthan Balachandar Thendral, visualization; David R. Sherwood, supervision, writing-original draft, funding acquisition, project administration.

Competing Interests

No competing interests declared for all authors

Author ORCID

Kieop Park https://orcid.org/0000-0002-6380-4730

Ranjay Jayadev https://orcid.org/0000-0003-0465-0337

Sara G. Payne https://orcid.org/0000-0002-3572-9112

Isabel Kenny-Ganzert https://orcid.org/0000-0001-6306-4472

Qiuyi Chi https://orcid.org/0000-0003-1297-4163

Daniel S. Costa https://orcid.org/0000-0003-2179-8800

Will Ramos-Lewis https://orcid.org/0000-0002-4627-4571

Siddharthan Balachandar Thendral https://orcid.org/0000-0002-4674-7033

David R Sherwood https://orcid.org/0000-0002-4448-6917

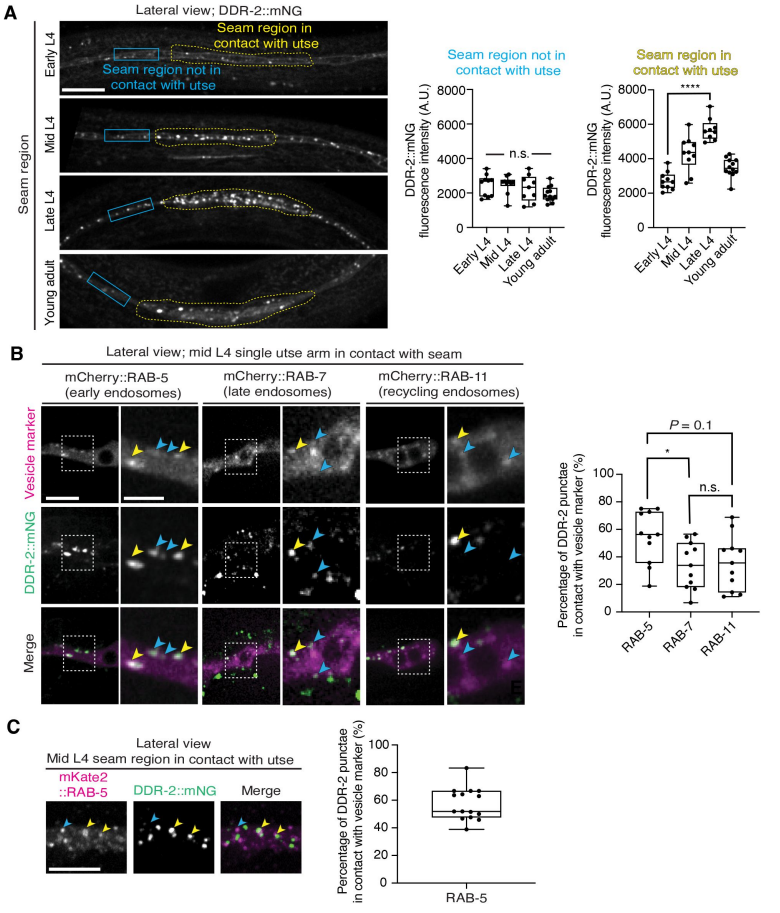

Figure 3—figure supplement 1

DDR-2 is found within endocytic vesicles.

Related to ***Figure 3***. (**A**) Lateral fluorescence images of DDR-2::mNG in the seam cells from the early L4 to young adult stages. Note that these images are the same animals as in ***Figure 3B*** with a larger cropped field of view to include regions of the seam not in contact with the utse. Quantification of mean fluorescence intensity in the blue and yellow boxed regions is shown on the right (n ≥ 9 all stages). Boxplots for yellow boxed regions are reproduced from ***Figure 3B***. n.s. (not significant), $P > 0.05$; Kruskal-Wallis *H* test. ****$P \leq 0.0001$, one-way ANOVA with post hoc Dunnett's test. (**B**) Lateral fluorescence images of DDR-2::mNG within a single arm of the utse tissue at the mid L4 stage, visualized together with mCherry-tagged RAB-5, RAB-7, or RAB-11. Boxed regions are magnified on the right. Yellow arrowheads denote DDR-2 punctae in contact with the respective vesicle marker, while blue arrowheads correspond to DDR-2 puncta that not in contact with vesicle markers. The boxplot shows quantification of percentage overlap of DDR-2 punctae with vesicle markers (n = 11 animals per marker). *$P \leq 0.05$, n.s. (not significant), $P > 0.05$; one-way ANOVA with post hoc Dunnett's T3 test. (**C**) Left: Lateral fluorescence images of DDR-2::mNG and mKate2::RAB-5 in the seam region contacting the utse. Arrowheads denote DDR-2 punctae in contact with (yellow) or not in contact with (blue) mCherry::RAB-5 punctae. Right: Percentage overlap of DDR-2 punctae with RAB-5 (n = 15). Scale bars, 20 µm. Box edges in boxplots represent the 25th and 75th percentiles, the line in the box denotes the median value, and whiskers mark the minimum and maximum values.

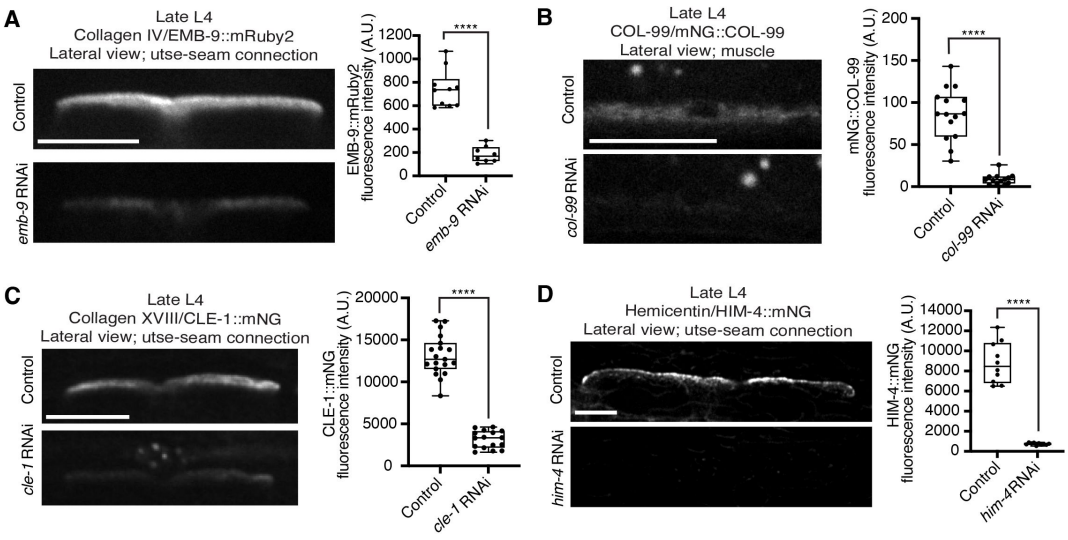

Figure 4—figure supplement 1

Collagen and hemicentin knockdown efficiencies.

Related to ***Figure 4***. (**A**) Lateral fluorescence images of EMB-9::mRuby2 (type IV collagen) at the utse-seam BM-BM connection in late L4 control or *emb-9* RNAi-treated animals. Mean fluorescence intensity quantified on the right (n ≥ 8 all treatments). (**B**) Lateral fluorescence images of mNG::COL-99 (COL-99) in the body wall muscle tissue in late L4 control or *col-99* RNAi-treated animals. Mean fluorescence intensity quantified on the right (n ≥ 13 all treatments). COL-99 signal in the muscle was analyzed as COL-99 was not detected at the utse-seam connection. (**C**) Lateral fluorescence images of CLE-1::mNG (type XVIII collagen) at the utse-seam BM-BM attachment in late L4 control or *cle-1* RNAi-treated animals. Mean fluorescence intensity quantified on the right (n ≥ 16 all treatments). (**D**) Lateral fluorescence images of HIM-4::mNG (hemicentin) at the utse-seam BM-BM connection in late L4 control or *him-4* RNAi-treated animals. Mean fluorescence intensity quantified on the right (n = 10 all treatments). ****$P \leq 0.0001$, unpaired two-tailed Student's *t* test (EMB-9, CLE-1, and HIM-4) or Mann-Whitney *U* test (COL-99). Scale bars, 20 µm. Box edges in boxplots represent the 25th and 75th percentiles, the line in the box denotes the median value, and whiskers mark the minimum and maximum values.

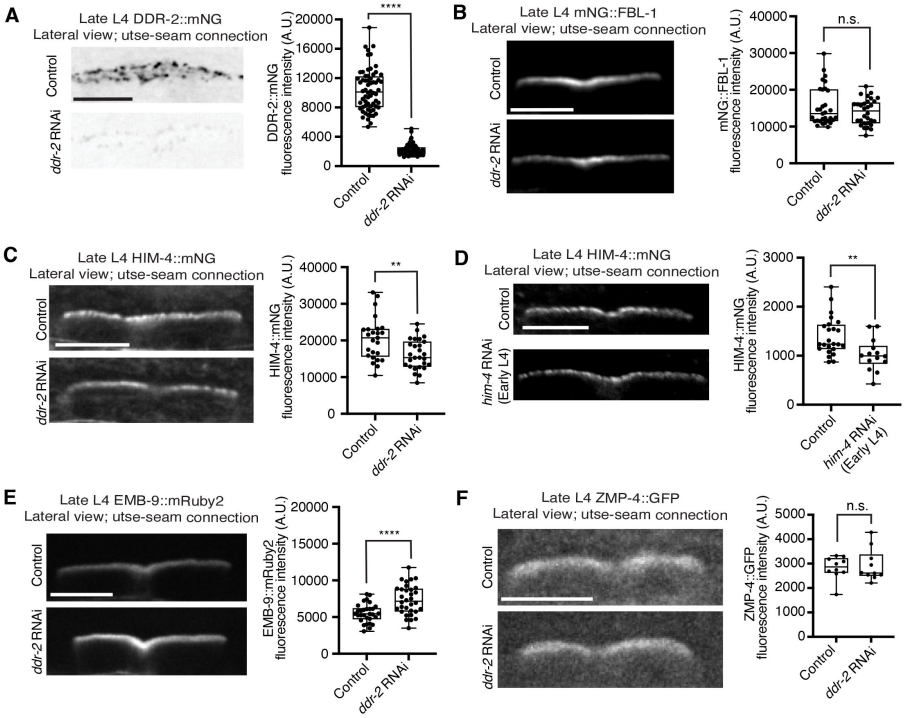

Figure 5—figure supplement 1

ddr-2 loss does not reduce functional levels of fibulin, hemicentin, type IV collagen, and matrix metalloproteinase ZMP-4 at the utse-seam connection.

Related to ***Figure 5***. (**A**) Lateral fluorescence images of DDR-2::mNG at the utse-seam BM-BM connection in late L4 control or *ddr-2* RNAi-treated animals. Mean fluorescence intensity quantified on the right (n ≥ 60 all treatments). ****$P \leq 0.0001$, Mann-Whitney *U* test. (**B**) Lateral fluorescence images of mNG::FBL-1 (fibulin) at the utse-seam connection in late L4 control or *ddr-2* RNAi-treated animals. Mean fluorescence intensity quantified on the right (n ≥ 30 all treatments). n.s. (not significant), $P > 0.05$, Mann-Whitney *U* test. (**C**) Lateral fluorescence images of HIM-4::mNG (hemicentin) at the utse-seam tissue linkage in late L4 control or *ddr-2* RNAi-treated animals. Mean fluorescence intensity quantified on the right (n ≥ 25 all treatments). **$P \leq 0.01$, unpaired two-tailed Student's *t* test.

(D) Lateral fluorescence images of HIM-4::mNG (hemicentin) at the utse-seam connection in late L4 control or *him-4* RNAi-treated animals. RNAi was initiated at the early L4 stage. Mean fluorescence intensity quantified on the right (n ≥ 14 all treatments). **$P \leq 0.01$, unpaired two-tailed Student's *t* test.

(E) Lateral fluorescence images of EMB-9::mRuby2 (type IV collagen) at the utse-seam attachment site in late L4 control or *ddr-2* RNAi-treated animals. Mean fluorescence intensity quantified on the right (n ≥ 30 all treatments). ****$P \leq 0.0001$, unpaired two-tailed Student's *t* test. (**F**) Lateral fluorescence images of matrix metalloproteinase ZMP-4::GFP at the utse-seam tissue connection in late L4 control or *ddr-2* RNAi-treated animals. Mean fluorescence intensity quantified on the right (n = 10 all treatments). n.s. (not significant), $P > 0.05$, Mann-Whitney *U* test. Scale bars, 20 μm. Box edges in boxplots represent the 25th and 75th percentiles, the line in the box denotes the median value, and whiskers mark the minimum and maximum values.

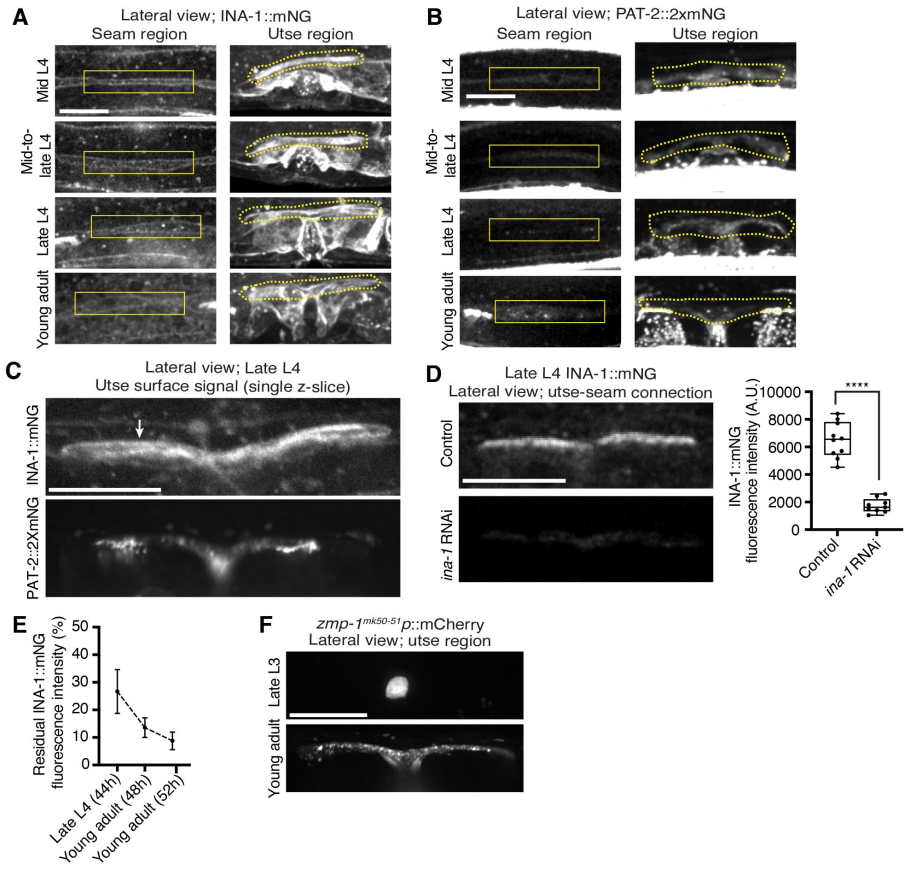

Figure 5—figure supplement 2

The integrin α subunits INA-1 and PAT-2 are localized within both the utse and seam cells.

Related to ***Figure 5***. (**A**) Lateral fluorescence z-projections of the integrin α subunit INA-1::mNG between the mid L4 and young adult stages. Localization in the seam and utse are indicated by solid and dotted boxed regions respectively (n ≥ 10 animals examined all stages). (**B**) Lateral fluorescence z-projections of the integrin α subunit PAT-2::2XmNG between the mid L4 and young adult stages. Localization in the seam and utse are indicated by solid and dotted boxed regions respectively (n ≥ 7 animals examined all stages). (**C**) Lateral fluorescence images of INA-1::mNG and PAT-2::2XmNG at the z-plane of the utse surface in late L4 animals (n ≥ 10 animals examined each). Arrow indicates strong INA-1 signal at the utse surface. (**D**) Lateral fluorescence images of INA-1::mNG at the utse-seam connection in late L4 control or *ina-1* RNAi-treated animals. Mean fluorescence intensity quantified on the right (n ≥ 9 all treatments). ****$P \leq 0.0001$, unpaired two-tailed Student's *t* test. (**E**) Quantification of residual INA-1::mNG fluorescence intensity at the utse-seam interface at the indicated developmental stages following *ina-1* knockdown initiated at the L1 stage. Data are represented as percentages of mean INA-1::mNG at the respective stages in control animals (n ≥ 7 animals examined all stages). Error bars denote SD. (**F**) Lateral fluorescence z-projections of mCherry driven by the *zmp-1*$^{mK50-51}$ promoter in the utse region in late L3 and young adult animals (n = 5 animals examined at each stage).

Figure 6—figure supplement 1

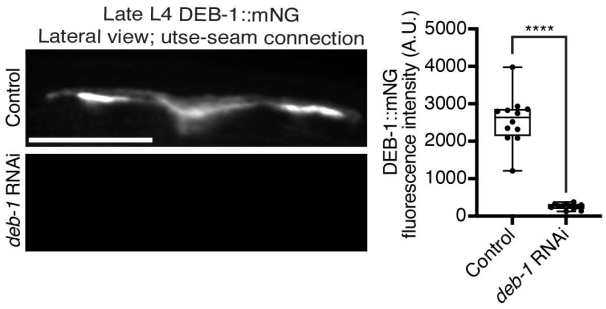

Figure 6—figure supplement 1

deb-1 knockdown efficiency.

Related to ***Figure 6***. Lateral fluorescence images of DEB-1::mNG (vinculin) at the utse-seam connection in late L4 control or *deb-1* RNAi-treated animals. Mean fluorescence intensity quantified on the right (n = 12 all treatments). ****$P \leq 0.0001$, unpaired two-tailed Student's *t* test. Scale bars, 20 µm. Box edges in boxplots represent the 25th and 75th percentiles, the line in the box denotes the median value, and whiskers mark the minimum and maximum values.

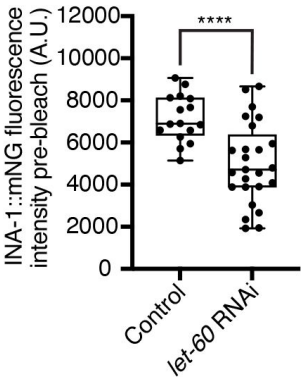

Figure 7—figure supplement 1

Ras/*let-60* knockdown reduces INA-1::mNG levels at the utse-seam connection.

Related to ***Figure 7***. Quantification of mean INA-1::mNG fluorescence intensity at the utse-seam connection prior to photobleaching in control or Ras/*let-60* RNAi-treated late L4 animals (see representative images in ***Figure 7B***, pre-bleach panel. Control n = 16; *let-60* RNAi n = 25. ****$P \leq 0.0001$, unpaired two-tailed Student's *t* test. Scale bars, 20 µm. Box edges in boxplots represent the 25th and 75th percentiles, the line in the box denotes the median value, and whiskers mark the minimum and maximum values.

References

Abrahamson D. R (1985) **Origin of the glomerular basement membrane visualized after in vivo labeling of laminin in newborn rat kidneys** *J Cell Biol* **100**:1988–2000

Altincicek B. , Fischer M. , Fischer M. , Luersen K. , Boll M. , Wenzel U. , Vilcinskas A. (2010) **Role of matrix metalloproteinase ZMP-2 in pathogen resistance and development in Caenorhabditis elegans** *Dev Comp Immunol* **34**:1160–1169

Bayer S. V. , Grither W. R. , Brenot A. , Hwang P. Y. , Barcus C. E. , Ernst M. , Pence P. , Walter C. , Pathak A. , Longmore G. D. (2019) **DDR2 controls breast tumor stiffness and metastasis by regulating integrin mediated mechanotransduction in CAFs** *Elife* **8**

Bays J. L. , DeMali K. A. (2017) **Vinculin in cell-cell and cell-matrix adhesions** *Cell Mol Life Sci* **74**:2999–3009

Bernadskaya Y. Y. , Brahmbhatt S. , Gline S. E. , Wang W. , Christiaen L. (2019) **Discoidin-domain receptor coordinates cell-matrix adhesion and collective polarity in migratory cardiopharyngeal progenitors** *Nat Commun* **10**

Borza C. M. , Bolas G. , Zhang X. , Browning Monroe M. B. , Zhang M. Z. , Meiler J. , Skwark M. J. , Harris R. C. , Lapierre L. A. , Goldenring J. R. , Hook M. , Rivera J. , Brown K. L. , Leitinger B. , Tyska M. J. , Moser M. , Bottcher R. T. , Zent R. , Pozzi A. (2022) **The Collagen Receptor Discoidin Domain Receptor 1b Enhances Integrin beta1-Mediated Cell Migration by Interacting With Talin and Promoting Rac1 Activation** *Front Cell Dev Biol* **10**

Borza C. M. , Pozzi A. (2014) **Discoidin domain receptors in disease** *Matrix Biol* **34**:185–192

Brown K. L. , Cummings C. F. , Vanacore R. M. , Hudson B. G. (2017) **Building collagen IV smart scaffolds on the outside of cells** *Protein Sci* **26**:2151–2161

Brown N. H (2011) **Extracellular matrix in development: insights from mechanisms conserved between invertebrates and vertebrates** *Cold Spring Harb Perspect Biol* **3**

Carney T. J. , Feitosa N. M. , Sonntag C. , Slanchev K. , Kluger J. , Kiyozumi D. , Gebauer J. M. , Coffin Talbot J. , Kimmel C. B. , Sekiguchi K. , Wagener R. , Schwarz H. , Ingham P. W. , Hammerschmidt M. (2010) **Genetic analysis of fin development in zebrafish identifies furin and hemicentin1 as potential novel fraser syndrome disease genes** *PLoS Genet* **6**

Castro-Sanchez L. , Soto-Guzman A. , Navarro-Tito N. , Martinez-Orozco R. , Salazar E. P. (2010) **Native type IV collagen induces cell migration through a CD9 and DDR1-dependent pathway in MDA-MB-231 breast cancer cells** *Eur J Cell Biol* **89**:843–852

Ceron J. , Rual J. F. , Chandra A. , Dupuy D. , Vidal M. , van den Heuvel S. (2007) **Large-scale RNAi screens identify novel genes that interact with the C. elegans retinoblastoma pathway as well as splicing-related components with synMuv B activity** *BMC Dev Biol* **7**

Chapman J. O. , Li H. , Lundquist E. A. (2008) **The MIG-15 NIK kinase acts cell-autonomously in neuroblast polarization and migration in C. elegans** *Dev Biol* **324**:245–257

Chastney M. R. , Conway J. R. W. , Ivaska J. (2021) **Integrin adhesion complexes** *Curr Biol* **31**

Chen L. , Kong X. , Fang Y. , Paunikar S. , Wang X. , Brown J. A. L. , Bourke E. , Li X. , Wang J. (2021) **Recent Advances in the Role of Discoidin Domain Receptor Tyrosine Kinase 1 and Discoidin Domain Receptor Tyrosine Kinase 2 in Breast and Ovarian Cancer** *Front Cell Dev Biol* **9**

Clay M. R. , Sherwood D. R. (2015) **Basement Membranes in the Worm: A Dynamic Scaffolding that Instructs Cellular Behaviors and Shapes Tissues** *Curr Top Membr* **76**:337–371

Conklin M. W. , Ada-Nguema A. , Parsons M. , Riching K. M. , Keely P. J. (2010) **R-Ras regulates beta1-integrin trafficking via effects on membrane ruffling and endocytosis** *BMC Cell Biol* **11**

Corcoran D. S. , Juskaite V. , Xu Y. , Gorlitz F. , Alexandrov Y. , Dunsby C. , French P. M. W. , Leitinger B. (2019) **DDR1 autophosphorylation is a result of aggregation into dense clusters** *Sci Rep* **9**

Dickinson D. J. , Ward J. D. , Reiner D. J. , Goldstein B. (2013) **Engineering the Caenorhabditis elegans genome using Cas9-triggered homologous recombination** *Nat Methods* **10**:1028–1034

Edelstein A. , Amodaj N. , Hoover K. , Vale R. , Stuurman N. (2010) **Computer control of microscopes using microManager** *Curr Protoc Mol Biol Chapter 14: Unit14 20*

Feitosa N. M. , Zhang J. , Carney T. J. , Metzger M. , Korzh V. , Bloch W. , Hammerschmidt M. (2012) **Hemicentin 2 and Fibulin 1 are required for epidermal-dermal junction formation and fin mesenchymal cell migration during zebrafish development** *Dev Biol* **369**:235–248

Fidler A. L. , Boudko S. P. , Rokas A. , Hudson B. G. (2018) **The triple helix of collagens - an ancient protein structure that enabled animal multicellularity and tissue evolution** *J Cell Sci* **131**

Frische E. W. , Pellis-van Berkel W. , van Haaften G. , Cuppen E. , Plasterk R. H. , Tijsterman M. , Bos J. L. , Zwartkruis F. J. (2007) **RAP-1 and the RAL-1/exocyst pathway coordinate hypodermal cell organization in Caenorhabditis elegans** *EMBO J* **26**:5083–5092

Frokjaer-Jensen C. , Davis M. W. , Ailion M. , Jorgensen E. M. (2012) **Improved Mos1-mediated transgenesis in C. elegans** *Nat Methods* **9**:117–118

Fu H. L. , Valiathan R. R. , Arkwright R. , Sohail A. , Mihai C. , Kumarasiri M. , Mahasenan K. V. , Mobashery S. , Huang P. , Agarwal G. , Fridman R. (2013) **Discoidin domain receptors: unique receptor tyrosine kinases in collagen-mediated signaling** *J Biol Chem* **288**:7430–7437

Gao Y. , Mruk D. , Chen H. , Lui W. Y. , Lee W. M. , Cheng C. Y. (2017) **Regulation of the blood-testis barrier by a local axis in the testis: role of laminin alpha2 in the basement membrane** *FASEB J* **31**:584–597

Ghosh S. , Sternberg P. W. (2014) **Spatial and molecular cues for cell outgrowth during C. elegans uterine development** *Dev Biol* **396**:121–135

Gianakas C. A. , Keeley D. P. , Ramos-Lewis W. , Park K. , Jayadev R. , Kenny I. W. , Chi Q. , Sherwood D. R. (2023) **Hemicentin-mediated type IV collagen assembly strengthens juxtaposed basement membrane linkage** *J Cell Biol* **222**

Gieseler K. , Qadota H. , Benian G. M. (2017) **Development, structure, and maintenance of C. elegans body wall muscle** *WormBook* **2017**:1–59

Goh L. K. , Sorkin A. (2013) **Endocytosis of receptor tyrosine kinases** *Cold Spring Harb Perspect Biol* **5**

Gross O. , Beirowski B. , Harvey S. J. , McFadden C. , Chen D. , Tam S. , Thorner P. S. , Smyth N. , Addicks K. , Bloch W. , Ninomiya Y. , Sado Y. , Weber M. , Vogel W. F. (2004) **DDR1-deficient mice show localized subepithelial GBM thickening with focal loss of slit diaphragms and proteinuria** *Kidney Int* **66**:102–111

Hagedorn E. J. , Yashiro H. , Ziel J. W. , Ihara S. , Wang Z. , Sherwood D. R. (2009) **Integrin acts upstream of netrin signaling to regulate formation of the anchor cell's invasive membrane in C. elegans** *Dev Cell* **17**:187–198

Hisamoto N. , Nagamori Y. , Shimizu T. , Pastuhov S. I. , Matsumoto K. (2016) **The C. elegans Discoidin Domain Receptor DDR-2 Modulates the Met-like RTK-JNK Signaling Pathway in Axon Regeneration** *PLoS Genet* **12**

Hohenester E. , Yurchenco P. D. (2013) **Laminins in basement membrane assembly** *Cell Adh Migr* **7**:56–63

Jayadev R. , Chi Q. , Keeley D. P. , Hastie E. L. , Kelley L. C. , Sherwood D. R. (2019) **alpha-Integrins dictate distinct modes of type IV collagen recruitment to basement membranes** *J Cell Biol* **218**:3098–3116

Jayadev R. , Morais M. , Ellingford J. M. , Srinivasan S. , Naylor R. W. , Lawless C. , Li A. S. , Ingham J. F. , Hastie E. , Chi Q. , Fresquet M. , Koudis N. M. , Thomas H. B. , O'Keefe R. T. , Williams E. , Adamson A. , Stuart H. M. , Banka S. , Smedley D. , C. Genomics England Research , Sherwood D. R. , Lennon R. (2022) **A basement membrane discovery pipeline uncovers network complexity, regulators, and human disease associations** *Sci Adv* **8**

Jayadev R. , Sherwood D. R. (2017) **Basement membranes** *Curr Biol* **27**

Juskaite V. , Corcoran D. S. , Leitinger B. (2017) **Collagen induces activation of DDR1 through lateral dimer association and phosphorylation between dimers** *Elife* **6**

Kamath R. S. , Ahringer J. (2003) **Genome-wide RNAi screening in Caenorhabditis elegans** *Methods* **30**:313–321

Keeley D. P. , Hastie E. , Jayadev R. , Kelley L. C. , Chi Q. , Payne S. G. , Jeger J. L. , Hoffman B. D. , Sherwood D. R. (2020) **Comprehensive Endogenous Tagging of Basement Membrane Components Reveals Dynamic Movement within the Matrix Scaffolding** *Dev Cell* **54**:60–74

Keeley D. P. , Sherwood D. R. (2019) **Tissue linkage through adjoining basement membranes: The long and the short term of it** *Matrix Biol* **75**:58–71

Kelley L. C. , Chi Q. , Caceres R. , Hastie E. , Schindler A. J. , Jiang Y. , Matus D. Q. , Plastino J. , Sherwood D. R. (2019) **Adaptive F-Actin Polymerization and Localized ATP Production Drive Basement Membrane Invasion in the Absence of MMPs** *Dev Cell* **48**:313–328

Kelley L. C. , Wang Z. , Hagedorn E. J. , Wang L. , Shen W. , Lei S. , Johnson S. A. , Sherwood D. R. (2017) **Live-cell confocal microscopy and quantitative 4D image analysis of anchor-cell invasion through the basement membrane in Caenorhabditis elegans** *Nat Protoc* **12**:2081–2096

Khoshnoodi J. , Pedchenko V. , Hudson B. G. (2008) **Mammalian collagen IV** *Microsc Res Tech* **71**:357–370

Lee M. , Cram E. J. , Shen B. , Schwarzbauer J. E. (2001) **Roles for beta(pat-3) integrins in development and function of Caenorhabditis elegans muscles and gonads** *J Biol Chem* **276**:36404–36410

Leitinger B (2014) **Discoidin domain receptor functions in physiological and pathological conditions** *Int Rev Cell Mol Biol* **310**:39–87

Lilja J. , Zacharchenko T. , Georgiadou M. , Jacquemet G. , De Franceschi N. , Peuhu E. , Hamidi H. , Pouwels J. , Martens V. , Nia F. H. , Beifuss M. , Boeckers T. , Kreienkamp H. J. , Barsukov I. L. , Ivaska J. (2017) **SHANK proteins limit integrin activation by directly interacting with Rap1 and R-Ras** *Nat Cell Biol* **19**:292–305

Martin-Bermudo M. D. , Brown N. H. (1999) **Uncoupling integrin adhesion and signaling: the betaPS cytoplasmic domain is sufficient to regulate gene expression in the Drosophila embryo** *Genes Dev* **13**:729–739

Merchant S. N. , Burgess B. J. , Adams J. C. , Kashtan C. E. , Gregory M. C. , Santi P. A. , Colvin R. , Collins B. , Nadol J. B. (2004) **Temporal bone histopathology in alport syndrome** *Laryngoscope* **114**:1609–1618

Mihai C. , Chotani M. , Elton T. S. , Agarwal G. (2009) **Mapping of DDR1 distribution and oligomerization on the cell surface by FRET microscopy** *J Mol Biol* **385**:432–445

Moerman D. G. , Williams B. D. (2006) **Sarcomere assembly in C. elegans muscle** *WormBook* :1–16

Mok D. Z. , Sternberg P. W. , Inoue T. (2015) **Morphologically defined sub-stages of C. elegans vulval development in the fourth larval stage** *BMC Dev Biol* **15**

Morrissey M. A. , Keeley D. P. , Hagedorn E. J. , McClatchey S. T. H. , Chi Q. , Hall D. H. , Sherwood D. R. (2014) **B-LINK: a hemicentin, plakin, and integrin-dependent adhesion system that links tissues by connecting adjacent basement membranes** *Dev Cell* **31**:319–331

Morrissey M. A. , Sherwood D. R. (2015) **An active role for basement membrane assembly and modification in tissue sculpting** *J Cell Sci* **128**:1661–1668

Murphy J. E. , Padilla B. E. , Hasdemir B. , Cottrell G. S. , Bunnett N. W. (2009) **Endosomes: a legitimate platform for the signaling train** *Proc Natl Acad Sci U S A* **106**:17615–17622

Naylor R. W. , Morais M. , Lennon R. (2021) **Complexities of the glomerular basement membrane** *Nat Rev Nephrol* **17**:112–127

Newman A. P. , White J. G. , Sternberg P. W. (1996) **Morphogenesis of the C. elegans hermaphrodite uterus** *Development* **122**:3617–3626

Pani A. M. , Goldstein B. (2018) **Direct visualization of a native Wnt in vivo reveals that a long-range Wnt gradient forms by extracellular dispersal** *Elife* **7**

Park J. O. , Pan J. , Mohrlen F. , Schupp M. O. , Johnsen R. , Baillie D. L. , Zapf R. , Moerman D. G. , Hutter H. (2010) **Characterization of the astacin family of metalloproteases in C. elegans** *BMC Dev Biol* **10**

Payne L. S. , Huang P. H. (2014) **Discoidin domain receptor 2 signaling networks and therapy in lung cancer** *J Thorac Oncol* **9**:900–904

Pozzi A. , Yurchenco P. D. , Iozzo R. V. (2017) **The nature and biology of basement membranes** *Matrix Biol* **57**:1–11

Rual J. F. , Ceron J. , Koreth J. , Hao T. , Nicot A. S. , Hirozane-Kishikawa T. , Vandenhaute J. , Orkin S. H. , Hill D. E. , van den Heuvel S. , Vidal M. (2004) **Toward improving Caenorhabditis elegans phenome mapping with an ORFeome-based RNAi library** *Genome Res* **14**:2162–2168

Sandri C. , Caccavari F. , Valdembri D. , Camillo C. , Veltel S. , Santambrogio M. , Lanzetti L. , Bussolino F. , Ivaska J. , Serini G. (2012) **The R-Ras/RIN2/Rab5 complex controls endothelial cell adhesion and morphogenesis via active integrin endocytosis and Rac signaling** *Cell Res* **22**:1479–1501

Sato K. , Norris A. , Sato M. , Grant B. D. (2014) **C. elegans as a model for membrane traffic** *WormBook* :1–47

Schindelin J. , Arganda-Carreras I. , Frise E. , Kaynig V. , Longair M. , Pietzsch T. , Preibisch S. , Rueden C. , Saalfeld S. , Schmid B. , Tinevez J. Y. , White D. J. , Hartenstein V. , Eliceiri K. , Tomancak P. , Cardona A. (2012) **Fiji: an open-source platform for biological-image analysis** *Nat Methods* **9**:676–682

Sherwood D. R. , Sternberg P. W. (2003) **Anchor cell invasion into the vulval epithelium in C. elegans** *Dev Cell* **5**:21–31

Singh N. , Han M. (1995) **sur-2, a novel gene, functions late in the let-60 ras-mediated signaling pathway during Caenorhabditis elegans vulval induction** *Genes Dev* **9**:2251–2265

Sixt M. , Engelhardt B. , Pausch F. , Hallmann R. , Wendler O. , Sorokin L. M. (2001) **Endothelial cell laminin isoforms, laminins 8 and 10, play decisive roles in T cell recruitment across the blood-brain barrier in experimental autoimmune encephalomyelitis** *J Cell Biol* **153**:933–946

Staudinger L. A. , Spano S. J. , Lee W. , Coelho N. , Rajshankar D. , Bendeck M. P. , Moriarty T. , McCulloch C. A. (2013) **Interactions between the discoidin domain receptor 1 and beta1 integrin regulate attachment to collagen** *Biol Open* **2**:1148–1159

Stiernagle T (2006) **Maintenance of C. elegans** *WormBook* :1–11

Suleiman H. , Zhang L. , Roth R. , Heuser J. E. , Miner J. H. , Shaw A. S. , Dani A. (2013) **Nanoscale protein architecture of the kidney glomerular basement membrane** *Elife* **2**

Taylor J. , Unsoeld T. , Hutter H. (2018) **The transmembrane collagen COL-99 guides longitudinally extending axons in C. elegans** *Mol Cell Neurosci* **89**:9–19

Timmons L. , Court D. L. , Fire A. (2001) **Ingestion of bacterially expressed dsRNAs can produce specific and potent genetic interference in Caenorhabditis elegans** *Gene* **263**:103–112

Timpl R. , Wiedemann H. , van Delden V. , Furthmayr H. , Kuhn K. (1981) **A network model for the organization of type IV collagen molecules in basement membranes** *Eur J Biochem* **120**:203–211

Tu H. , Huhtala P. , Lee H. M. , Adams J. C. , Pihlajaniemi T. (2015) **Membrane-associated collagens with interrupted triple-helices (MACITs): evolution from a bilaterian common ancestor and functional conservation in C. elegans** *BMC Evol Biol* **15**

Unsoeld T. , Park J. O. , Hutter H. (2013) **Discoidin domain receptors guide axons along longitudinal tracts in C. elegans** *Dev Biol* **374**:142–152

Villasenor R. , Kalaidzidis Y. , Zerial M. (2016) **Signal processing by the endosomal system** *Curr Opin Cell Biol* **39**:53–60

Vogel B. E. , Hedgecock E. M. (2001) **Hemicentin, a conserved extracellular member of the immunoglobulin superfamily, organizes epithelial and other cell attachments into oriented line-shaped junctions** *Development* **128**:883–894

Vogel W. F. , Abdulhussein R. , Ford C. E. (2006) **Sensing extracellular matrix: an update on discoidin domain receptor function** *Cell Signal* **18**:1108–1116

Walser M. , Umbricht C. A. , Frohli E. , Nanni P. , Hajnal A. (2017) **beta-Integrin de-phosphorylation by the Density-Enhanced Phosphatase DEP-1 attenuates EGFR signaling in C. elegans** *PLoS Genet* **13**

Welcker D. , Stein C. , Feitosa N. M. , Armistead J. , Zhang J. L. , Lutke S. , Kleinridders A. , Bruning J. C. , Eming S. A. , Sengle G. , Niehoff A. , Bloch W. , Hammerschmidt M. (2021) **Hemicentin-1 is an essential extracellular matrix component of the dermal-epidermal and myotendinous junctions** *Sci Rep* **11**

Wildwater M. , Sander N. , de Vreede G. , van den Heuvel S. (2011) **Cell shape and Wnt signaling redundantly control the division axis of C. elegans epithelial stem cells** *Development* **138**:4375–4385

Xiao Q. , Jiang Y. , Liu Q. , Yue J. , Liu C. , Zhao X. , Qiao Y. , Ji H. , Chen J. , Ge G. (2015) **Minor Type IV Collagen alpha5 Chain Promotes Cancer Progression through Discoidin Domain Receptor-1** *PLoS Genet* **11**

Xu H. , Bihan D. , Chang F. , Huang P. H. , Farndale R. W. , Leitinger B. (2012) **Discoidin domain receptors promote alpha1beta1- and alpha2beta1-integrin mediated cell adhesion to collagen by enhancing integrin activation** *PLoS One* **7**

Yochem J. , Herman R. K. (2003) **Investigating C. elegans development through mosaic analysis** *Development* **130**:4761–4768

Zhang Z. , Vuori K. , Wang H. , Reed J. C. , Ruoslahti E. (1996) **Integrin activation by R-ras** *Cell* **85**:61–69

Author information

Kieop Park
Department of Biology, Duke University, Box 90338, Durham, NC 27708, USA

Ranjay Jayadev
Department of Biology, Duke University, Box 90338, Durham, NC 27708, USA
ORCID iD: 0000-0003-0465-0337

Sara G. Payne
Department of Biology, Duke University, Box 90338, Durham, NC 27708, USA, Department of Cell Biology, Duke University Medical Center, Durham, NC 27708, USA

Isabel W. Kenny-Ganzert
Department of Biology, Duke University, Box 90338, Durham, NC 27708, USA

Qiuyi Chi
Department of Biology, Duke University, Box 90338, Durham, NC 27708, USA

Daniel S. Costa
Department of Biology, Duke University, Box 90338, Durham, NC 27708, USA

William Ramos-Lewis
Department of Biology, Duke University, Box 90338, Durham, NC 27708, USA

Siddharthan Balachandar Thendral
Department of Biology, Duke University, Box 90338, Durham, NC 27708, USA

David R. Sherwood
Department of Biology, Duke University, Box 90338, Durham, NC 27708, USA
For correspondence: david.sherwood@duke.edu
ORCID iD: 0000-0002-4448-6917

Editors

Reviewer #1 (Public Review):

Park et al demonstrate that cells on either side of a BM-BM linkage strengthen their adhesion to that matrix using a positive feedback mechanism involving a discoidin domain receptor (DDR-2) and integrin (INA-1 + PAT-3). In response to its extracellular ligand (Collagen IV/EMB-9), DDR-2 is endocytosed and initiates signaling that in turn stabilizes integrin at the membrane. DDR-2 signaling operates via Ras/LET-60. This work's strength lies in its excellent in vivo imaging, especially of endogenously tagged proteins. For example, tagged DDR-2:mNG could be seen relocating from seam cell membranes to endosomes. I also think a second strength of this system is the ability to chart the development of BM-BM linkage over time based on the stages of worm larval development. This allows the authors to show DDR signaling is needed to establish linkage, rather than maintain it. It likely is relevant to many types of cells that use integrin to adhere to BM and left me pondering a number of interesting questions. For example: (1) Does DDR-2 activation require integrin? Perhaps integrin gets the process started and DDR-2 positively reinforces that (conversely is DDR-2 at the top of a linear pathway)? (2) In ddr-2(qy64) mutants, projections seem to form from the central portion of the utse cell. Does this reveal a second function for DDR-2, regulating perhaps the cytoskeleton? And (3) can you use the forward genetic tools available in C. elegans to find new genes connecting DDR-2 and integrin? The authors discuss these ideas in their response to the reviews, and I look forward to hearing about their future work on these questions.

I do see two areas where the manuscript could be improved. First, the authors rely on imprecise genetic methods to reach their conclusions (i.e. systemic RNAi, or expression of dominant negative constructs.) I think their conclusion would be stronger if they used tissue specific degradation to block ddr-2 function specifically in the utse or seam cells. Methods to do this are now regularly used in C. elegans and the authors have already developed the necessary tissue-specific promoters. Second, the manuscript is presented in the introduction as a study on formation and function of BM-BM linkage. However, their results actually demonstrate a mechanism by which cells adhere to BM. Since ddr-2 appears to function equally in both utse + seam cells (based on their dominant negative data), there are likely three layers of adhesion (utse-BM, BM-BM, BM-seam) and if any of those break down, you get a partially penetrant rupture phenotype. I pointed this out in my initial review, and after reading the revised manuscript, I do still feel the authors' introduction presents the paper as dealing with how basement membranes link together. But, I wonder if this might this be a

question of terminology/language use? Maybe I am operating on a strict definition of linkage, and the authors use it more inclusively. What term(s) should we use to differentiate two basement membranes that are linked together, versus tissues that are connected through a basement membrane linkage? This is something that could be clarified in future publications.

These concerns do not undercut the significance of this work, which identifies an interesting mechanism cells use to strengthen adhesion during BM linkage formation. In fact, I am excited to read future papers detailing the connection between DDR-2 and integrin. But before undertaking those experiments the authors should be certain which cells require DDR-2 activity, and that should not be determined based solely on mis expression of a dominant negative.

Reviewer #2 (Public Review):

This paper explores the mechanisms by which cells in tissues use the extracellular matrix (ECM) to reinforce and establish connections. This is a mechanistic and quantitative paper that uses imaging and genetics to establish that the Type IV collagen, DDR-2/collagen receptor discoidin domain receptor 2, signaling through Ras to strengthen an adhesion between two cell types in C. elegans. This connection needs to be strong and robust to withstand the pressure of the numerous eggs that pass through the uterus. The major strengths of this paper are in crisply designed and clear genetic experiments, beautiful imaging, and well supported conclusions. I find very few weaknesses, although, perhaps the evidence that DDR-2 promotes utse-seam linkage through regulation of MMPs could be stronger. This work is impactful because it shows how cells in vivo make and strengthen a connection between tissues through ECM interactions involving collaboration between discoidin and integrin.

Author Response:

The following is the authors' response to the original reviews.

We have now incorporated the changes recommended by the reviewers to improve the interpretations and clarity of the manuscript. We are grateful for their thoughtful comments and suggestions, which have significantly strengthened the manuscript.

> ### *Reviewer #1 (Public Review):*
>
> *Park et al demonstrate that cells on either side of a BM-BM linkage strengthen their adhesion to that matrix using a positive feedback mechanism involving a discoidin domain receptor (DDR-2) and integrin (INA-1 + PAT-3). In response to its extracellular ligand (Collagen IV/EMB-9), DDR-2 is endocytosed and initiates signaling that in turn stabilizes integrin at the membrane. DDR-2 signaling operates via Ras/LET-60. This work's strength lies in its excellent in vivo imaging, especially of endogenously tagged proteins. For example, tagged DDR-2:mNG could be seen relocating from seam cell membranes to endosomes. I also think a second strength of this system is the ability to chart the development of BM-BM linkage over time based on the stages of worm larval development. This allows the authors to show DDR signaling is needed to establish linkage, rather than maintain it. It likely is relevant to many types of cells that use integrin to adhere to BM and left me pondering a number of interesting questions.*

We thank the reviewer for highlighting the strengths and impact of our work in expanding our understanding of tissue linkages and how DDR and integrins might work in other contexts.

> *For example: (1) Does DDR-2 activation require integrin? Perhaps integrin gets the process started and DDR-2 positively reinforces that (conversely is DDR-2 at the top of a linear pathway)?*

DDR activation by receptor clustering upon exposure to its ligand collagen is well documented (Juskaite et al., 2017 *eLife* PMID: 285ti0245). Clustered DDR is rapidly internalized into endocytic vesicles, where full activation of tyrosine kinase activity is thought to occur (Fu et al., 2013 *J Biol Chem* PMID: 23335507). Supporting this model, we found that concentrated type IV collagen is required for vesicular DDR-2 localization in the utse and seam cells at the utse-seam connection. Whether DDR-2 activation requires integrin has not been fully established. However, one study using mouse and human cell lines showed that DDR1 activation occurs independent of integrin (Vogel et al., 2000 *J Biol Chem* PMID: 10681566), consistent with the latter possibility raised by the reviewer that DDR-2 is upstream of integrin.

To test these hypotheses, we require an experimental condition where loss or near complete loss of INA- 1 integrin is achieved by the mid-to-late L4 larval stage, when DDR-2 is activated by collagen and taken into endocytic vesicles. Currently, we can only partially deplete INA-1 by RNAi (Figure 5—figure supplement 2E), and strong loss of function mutations in *ina-1* result in early larval arrest and lethality (Baum and Garriga, 1titi7 *Neuron* PMID: ti247263). To overcome these obstacles, we are adapting the new FLP-ON::TIR1 system developed for precise spatiotemporal protein degradation in worms (Xiao et al., 2023 *Genetics* PMID: 36722258). We hope to achieve a near complete knockdown of *ina-1* with this timed depletion strategy. In the future, we will use this system to block DDR-2 and integrin function specifically in the utse or seam cells, to complement our current dominant negative mis-expression approach.

> *(2) In ddr-2(qy64) mutants, projections seem to form from the central portion of the utse cell. Does this reveal a second function for DDR-2, regulating perhaps the cytoskeleton?*

We thank the reviewer for their observation and agree with their interpretation. We think it is important to comment on this and have stated in the results text, lines 208-212: “In addition, membrane projections emanating from the central body of the utse were detected in *ddr-2(qy64)* animals. These projections were first observed at the mid L4 stage and persisted to young adulthood (Figure 2C). These observations suggest that DDR-2 functions around the mid L4 to late L4 stages to promote utse-seam attachment, and that DDR-2 may also regulate utse morphology.”

> *And (3) can you use the forward genetic tools available in C. elegans to find new genes connecting DDR-2 and integrin?*

This is an excellent suggestion. We found that loss of *ddr-2* strongly enhanced the uterine prolapse (Rup) defect caused by RNAi mediated depletion of integrin. To find new genes connecting DDR-2 and integrin, a targeted screen for the Rup phenotype could be performed in an integrin reduction of function condition. As we cannot work with null or strong loss-of-function *ina-1* alleles (described above), the screen could be conducted with either timed depletion of INA-1 with candidate RNAi treatments, or combinatorial *ina-1* RNAi with candidate RNAi treatments.

> *I do see two areas where the manuscript could be improved. First, the authors rely on imprecise genetic methods to reach their conclusions (i.e. systemic RNAi, or expression of dominant negative constructs.) I think their conclusion would be stronger if they used tissue specific degradation to block ddr-2 function specifically in the utse or seam cells. Methods to do this are now regularly used in C. elegans and the authors have already developed the necessary tissue-specific promoters.*

We agree with the reviewer that tissue specific degradation of DDR-2 in the utse and seam cells will complement and strengthen our evidence for the site of action of DDR-2. As

described earlier, we are currently adapting the FLP-ON::TIR1 tissue degradation system to perform these experiments and will provide our findings in a follow-up manuscript.

> *Second, the manuscript is presented in the introduction as a study on formation and function of BM-BM linkage. The authors start the discussion in a similar manner. But their results are about adhesion between cells and BM. In fact they show the BM-BM linkage forms normally in ddr-2 mutants. Thus it seems like what they have really uncovered is an adhesion mechanism that works in parallel to the BM-BM linkage. Since ddr-2 appears to function equally in both utse + seam cells (based on their dominant negative data), there are likely three layers of adhesion (utse-BM, BM-BM, BM-seam) and if any of those break down, you get a partially penetrant rupture phenotype.*

The reviewer raises an important and interesting point, and we agree that we did not articulate the organization of the utse-seam tissue connection clearly. The utse-seam connection is comprised of the utse and seam BMs each ~50nm thick, and a connecting matrix bridging the two BMs, which is ~100nm thick (Vogel and Hedgecock, 2001 *Development* PMID: 11222143). Type IV collagen builds up to high levels within the connecting matrix and links the utse and seam BMs, and its concentration is required for DDR-2 vesiculation. An important point we did not highlight is that type IV collagen is approximately 400 nm long (Timpl et al. 1ti81, *Eur J Biochem* PMID: 6274634). Thus, collagen molecules within the connecting matrix could span the entire length of the utse-seam connection and project into the utse and seam BMs to interact with cell surface receptors. Consistent with this possibility, we found that buildup of type IV collagen that spans the utse-seam BM-BM linkage correlated with the timing of DDR-2 activation/vesiculation within utse and seam cells. In addition, super-resolution imaging of the mouse kidney glomerular basement membrane (GBM), a tissue connection between endothelial BM and epithelial (podocyte) BM, showed type IV collagen, which spans the BMs, projects into the endothelial and podocyte BMs (Suleiman et al., 2013 eLife PMID: 24137544). We carefully considered these points to generate the schematics in Figure 1A and Figure 8, but failed to articulate this point in the manuscript. We are grateful for the reviewer for bringing up our error and have now stated these details in the text to address the reviewer's concern as outlined below.

In the introduction (lines ti3-ti6): "A BM-BM tissue connection between the large, multinucleated uterine utse cell and epidermal seam cells stabilizes the uterus during egg laying. The utse-seam connection is formed by BMs of the utse and the seam cells, each ~50 nm thick, which are bridged by an ~100 nm connecting matrix (Vogel and Hedgecock 2001, Morrissey, Keeley et al. 2014, Gianakas, Keeley et al. 2023)."

In the discussion (lines 507-520): "We also found that internalization of DDR-2 at the utse-seam connection correlated with the assembly of type IV collagen at the BM-BM linkage and was dependent on type IV collagen deposition. Type IV collagen is ~400 nm in length and the utse-seam connecting matrix spans ~100 nm, while the utse and seam BMs are each ~50 nm thick (Timpl, Wiedemann et al. 1ti81, Vogel and Hedgecock 2001). Thus, collagen molecules in the connecting matrix could project into the utse and seam BMs to interact with DDR-2 on cell surfaces. Consistent with this possibility, super- resolution imaging of the mouse kidney glomerular basement membrane (tiBM), a tissue connection between podocytes and endothelial cells, showed type IV collagen within the tiBM projecting into the podocyte and endothelial BMs (Suleiman, Zhang et al. 2013). As DDR-2 is activated by ligand-induced clustering of the receptor (Juskaite, Corcoran et al. 2017, Corcoran, Juskaite et al. 201ti), it suggests that the BM-BM linking type IV collagen network, which is specifically assembled at high levels, clusters and activates DDR-2 in the utse and seam cells to coordinate cell-matrix adhesion at the tissue linkage site."

> *These concerns do not undercut the significance of this work, which identifies an interesting mechanism cells use to strengthen adhesion during BM linkage formation. In fact, I am excited to read future papers detailing the connection between DDR-2 and integrin. But before undertaking those experiments the authors should be certain which cells require DDR-2 activity, and that should not be determined based solely on mis expression of a dominant negative.*

We thank the reviewer for recognizing the significance of our work and reiterate that we will use tissue-specific degradation for site of action experiments in future studies on the biology of the utse- seam tissue linkage.

Reviewer #2 (Public Review):

> *This paper explores the mechanisms by which cells in tissues use the extracellular matrix (ECM) to reinforce and establish connections. This is a mechanistic and quantitative paper that uses imaging and genetics to establish that the Type IV collagen, DDR-2/collagen receptor discoidin domain receptor 2, signaling through Ras to strengthen an adhesion between two cell types in C. elegans. This connection needs to be strong and robust to withstand the pressure of the numerous eggs that pass through the uterus. The major strengths of this paper are in crisply designed and clear genetic experiments, beautiful imaging, and well supported conclusions. I find very few weaknesses, although, perhaps the evidence that DDR-2 promotes utse-seam linkage through regulation of MMPs could be stronger. This work is impactful because it shows how cells in vivo make and strengthen a connection between tissues through ECM interactions involving collaboration between discoidin and integrin.*

We appreciate the reviewer's assessment of the impact of our work in detailing a mechanism for how cells increase their adhesion to the ECM to establish connections between adjacent tissues. We have softened the interpretation of our MMP localization data to address the reviewer's concern (detailed below).

Reviewer #1 (Recommendations For The Authors):

> *Regarding Figure 1D, is it possible to show when the BM forms on the cartoons more clearly (something like the 3rd section of Fig 3A)? I can see it in the timeline but it's hard to follow in the diagrams.*

We agree with the reviewer that we could show when the BM-BM connecting matrix forms more clearly in Figure 1D. Hemicentin and fibulin, the earliest components of the connecting matrix, are detected at very low levels at the utse-seam connection during the mid-L4 stage and are more prominently localized by the mid-to-late L4 stage (Gianakas et al., 2023 *J Cell Biol* PMID: 36282214). For this reason, we only show the connecting matrix in yellow from the mid-to-late L4 stages onward. We have now made the BM-BM connection more prominent in the figure 1D cartoons with boxed outlines (similar to Figure 3A as the reviewer suggested). We also added a label for the time window when the BM-BM connection forms.

> *Regarding the RNAi induced prolapse phenotype, looking at 2B, it appears that between 5% and 10% of animals have uterine prolapse when fed control RNAi. Is this correct, it seems very high? This prolapse in control animals was not observed other RNAi experiments such as Figure 5C.*

We thank the reviewer for pointing this out. For Figure 2B, the control used was wild-type N2 animals fed with OP50 *E. coli* bacteria, rather than HT115 bacteria carrying the L4440 empty vector (control RNAi). This is because the main comparisons were to five *ddr-1* and *ddr-2* mutant strains. We did notice a slightly higher baseline uterine prolapse frequency (5% on average, detailed in Figure 2—Source data 1) in wild-type animals fed OP50 bacteria, compared to HT115 bacteria fed animals (approximately 1-2% on average). It is possible this

could be linked to the nutritional differences in the two bacterial strains. However, we are confident of our data in Figure 2B as we carried out 3 independent trials, and the uterine prolapse frequencies in *ddr-1* mutant animals matched the baseline in wild-type animals, while the frequencies for *ddr-2* mutants were all increased over the baseline in all trials (as detailed in Figure 2—Source data 1).

> *Relating to the point above, in reading the methods to try to understand how they did the RNAi, I noticed that they measure prolapse continually over five days. I didn't realize it takes a long time to occur. I think they should explain this in the text and in the figures. Reading the manuscript I thought prolapse occurred as soon as mutant animals began laying eggs. In the text they should explain this when they first assay the phenotype (page 7), and for figures the Y axis on the graphs could say "% uterine prolapse after 5 days."*

We thank the reviewer for their suggestions. We did not articulate clearly that the utse-seam connection is able to withstand some mechanical stress, even when key components are lost. It's only over time and repeated use that the connection breaks down. This is likely because a number of components contribute to the connection and as we have shown previously, there is feedback, such that when one components is reduced, such as collagen, hemicentin is increased in levels at the BM-BM connection. Since ruptures arising from utse-seam detachments typically occur sometime after the onset

of egg-laying, we screened the entire egg-laying period (days two to five post-L1) as described in Gianakas et al. 2023. We have now incorporated these points in the text and figures as follows:

In the introduction, we clarified that utse-seam BM-BM connection breaksdown over time, by adding (lines titi-105): "Hemicentin promotes the recruitment of type IV collagen, which accumulates at high levels at the BM-BM tissue connection and strengthens the adhesion, allowing it to resist the strong mechanical forces of egg-laying. The utse-seam connection is robust, with each component of the tissue- spanning matrix contributing to the BM-BM connection (Gianakas, Keeley et al. 2023). This likely accounts for the ability of the utse-seam connection to initially resist mechanical forces after loss of any one of these components, delaying the uterine prolapse phenotype until sometime after the initiation of egg-laying."

We expanded the results text when we first describe the Rup phenotype (lines 183-184): "We first screened for the Rup phenotype caused by uterine prolapse, observing animals every day during the egg-laying period, from its onset (48 h post-L1) to end (120 h) (Methods)".

We provided more detail in the Methods section (lines 784-7ti0): "Uterine prolapse frequency was assessed as described previously (Gianakas et al 2023). Briefly, synchronized L1 larvae were plated (~20 animals per plate) and after 24 h, the exact number of worms on each plate was recorded. Plates were then visually screened for ruptured worms (uterine prolapse) every 24 h during egg-laying (between 48 h to 120 h post-L1). We chose to examine the entire egg-laying period as ruptures arising from utse-seam detachments do not usually occur at the onset of egg-laying, but after cycles of egg-laying that place repeated mechanical stress on the utse-seam connection (Gianakas et al 2023)."

Finally, we modified the Y-axes of graphs in Figure 2B and 5C and the respective figure legends as suggested by the reviewer.

> *Then I went back and compared to the previous publication (Gianakas, 2023). I would be interested to see a time course of how many animals prolapse after 1 day, 2 days, etc.? Is this consistent with their data on hemicentrin?*

We agree with the reviewer that a time course of uterine prolapse would be interesting as we saw ruptures occur throughout the egg-laying period. However, for the hemicentin

knockdown experiments in Gianakas et al. 2023 as well as the experiments in this study, we recorded only the pooled number of animals with ruptures at the end of the experimental window. In future studies we will also record the uterine prolapse frequencies on each day to generate time courses that will provide more insight into the function of proteins at the utse-seam connection.

> *Lines 183-184: I'm not sure what it means to say "trended towards displaying a significant Rup phenotype?" Since the difference was not statistically significant, it would be better to say something like "increased but not statistically significant."*

We agree with the reviewer and have now modified this sentence (lines 190-193): “Animals carrying the *ddr-2(ok574)* allele, which deletes a portion of the intracellular kinase domain (Unsoeld, Park et al. 2013),also showed an increased frequency of the Rup phenotype compared to wild-type animals, although this difference was not statistically significant (Figure 2A and B)”.

> *Line 186: 'penetrant' needs a qualifier to indicate the magnitude of the proportion of individuals with the phenotype.*

As we provide the Rup frequency numbers in Figure 2—Source data 1, we modified the sentence as follows (lines 1ti3-1ti5): “We further generated a full-length *ddr-2* deletion allele, *ddr-2(qy64)*, and confirmed that complete loss of *ddr-2* led to a significant uterine prolapse defect (Figure 2A and B).”

> *Lines 206-208; could the mounting/imaging procedure (which I assume requires squeezing the worm between agarose pad and coverslip) alter the occurrence of prolapse? I would think prolapse would occur more frequently under these conditions as compared to worms laying eggs on a plate.*

The reviewer brings up an important concern. The mounting and imaging procedure does require placing the worm between an agarose pad and a coverslip. However, this did not alter the occurrence of uterine prolapse in this experiment. We were careful to perform the same procedure on both wild-type and *ddr- 2(qy64)* animals to control for this. As detailed in the manuscript, none of the eight wild-type animals we mounted underwent uterine prolapse after recovery off the coverslip, and among the *ddr-2(qy64)* mutants we mounted, only the ones that exhibited utse-seam detachments went on to rupture later.

We articulated these points more clearly by modifying lines 214-216 as follows: “Wild-type and *ddr- 2(qy64)* animals were mounted and imaged at the L4 larval stage for utse-seam attachment defects, recovered, and tracked to the 72-hour adult stage, where they were examined for the Rup phenotype.”

> *In seam cells you can see that DDR-2:mNG is present at membranes from early to mid L4, which makes sense. But I cannot see it on the membrane at any time point in the utse. Perhaps it is obscured by the yellow dotted line. Should it be visible on utse membranes before it is endocytosed?*

The reviewer raises an interesting question. We think it is likely that DDR-2 is initially on the membrane of the utse like it is on the seam cells. However, we have not observed this, possibly due to the complex shape and thin membrane extensions of the utse. We are unable even to detect clear membrane enrichment of membrane markers in the utse (for example, compare the utse and seam membrane markers in Figure 3B). Thus, we refrained from speculating on DDR-2 utse membrane localization in the manuscript, and instead focused on the pattern of vesicular DDR-2 peaking at the late L4 stage, which was clearly visible in both the utse and seam cells.

> *Sup Fig 3A - please show quantification of seam cells not contacting utse at the same Y-axis scale as for regions that do contact utse.*

We have modified the Y-axis scale for the quantification of the seam region not contacting the utse.

> *Figure 4A - I don't see a difference between WT and ok574 - what am I missing?*

In the representative *ok574* animal shown, a portion of the utse arm on the top right is detached from the seam. To make this phenotype clearer, we have recropped the image panels, readjusted the brightness and contrast of the utse and the seam, and redrawn the outline of the detachment to make this clearer.

> *Figure 4C+D, and lines 296-298: I'd bet that both are needed to recruit DDR-2 to membranes. But him-4 has a more severe phenotype because the RNAi knockdown is much more effective (perhaps b/c they are using the newer t444t vector).*

We agree with the reviewer that the *him-4* knockdown phenotype is likely more severe than *emb-9* knockdown. Type IV collagen at the utse-seam connection is very stable compared to hemicentin (Gianakas et al 2023, *J Cell Biol* PMID: 36282214, see Fig. 5C), which could explain the lower knockdown efficiency.

We modified our interpretation of the data in the text as follows (lines 308-312): “In addition, we did not detect DDR-2 at the cell surface, suggesting that hemicentin has a role in recruiting DDR-2 to the site of utse-seam attachment. It is possible that collagen could also function in DDR-2 recruitment, but we could not assess this definitively due to the lower knockdown efficiency of *emb-9* RNAi (Figure 4—figure supplement 1A).”

Reviewer #2 (Recommendations For The Authors):

> *Line 218 DDR-2 (typo)*

We have corrected this typo.

> *Evidence (line 344-348) may not be strong enough to say whether or not DDR-2 promotes utse-seam linkage through regulation of MMPs.*

We agree with the reviewer and have softened our conclusions as follows (lines 356-363): “The C. elegans genome harbors six MMP genes, named zinc metalloproteinase 1-6 (zmp-1-6) (Altincicek, Fischer et al. 2010). We examined four available reporters of ZMP localization (ZMP-1::tiFP, ZMP-2::tiFP, ZMP-3::tiFP, and ZMP-4::tiFP) (Kelley, Chi et al. 201ti).Only ZMP-4 was detected at the utse-seam connection and its localization was not altered by knockdown of *ddr-2* (Figure 5—figure supplement 1F). These observations suggest that DDR-2 does not promote utse-seam linkage through regulation of MMPs, although we cannot rule out roles for DDR-2 in promoting the expression or localization of ZMP-5 or ZMP-6.”

> *The authors show the critical period is in late L4, however, is the signaling needed later too? For example, is the linkage strengthening moderated by DDR-2 important as more eggs accumulate?*

The reviewer raises an interesting question. We observed that the vesicular localization of DDR-2 sharply declined before the onset of egg-laying. By young adulthood, very few punctate structures of DDR-2 were observed in the seam cells, and none in the utse (Figure 3B). Furthermore, the frequency of utse- seam detachments in *ddr-2* mutant animals peaked by the late L4 stage and did not increase after this time, suggesting DDR function is no longer required after the late L4 stage (Figure 2D). Thus, we believe that DDR-2 signaling strengthens

tissue linkage only during the early formation of the utse-seam connection between the mid and late L4 stage.

We incorporated these points in the discussion (lines 477-485): “Through analysis of genetic mutations in the *C. elegans* receptor tyrosine kinase (RTK) DDR-2, an ortholog to the two vertebrate DDR receptors (DDR1 & DDR2) (Unsoeld, Park et al. 2013), we discovered that loss of *ddr-2* results in utse-seam detachment beginning at the mid L4 stage. The frequency of detachments in *ddr-2* mutant animals peaked around the late L4 stage and did not increase after this time. This correlated with the levels of DDR-2::mNG at the utse-seam connection, which peaked at the late L4 stage and then sharply declined by adulthood. Together, these findings suggest that DDR-2 promotes utse-seam attachment in the early formation of the tissue connection between the mid and late L4 stage.”

> *Fig. 3B is the fluorescence quantification normalized to the area?*

Yes, it is. We used mean fluorescence intensity for all fluorescence quantifications to normalize for the area where the signal was measured. We added a line in Methods to emphasize this (lines 73ti-740): “We measured mean fluorescence intensity for all quantifications in order to account for linescan area.”

> *Fig. 4B a statistical assessment of the degree of co-localization of DDR-2::mNG and the endosomal markers might be a nice addition.*

We believe the reviewer is referring to Figure 3—figure supplement 1B. We have now added the statistical assessment of the degree of co-localization of DDR-2::mNG and the endosomal markers.

We want to sincerely thank the two reviewers for their thoughtful comments and suggestions. The changes we have made in response to these comments have substantially improved the manuscript.